EPFL

KTH
VETENSKAP
OCH KONST

Politecnico di Torino
1859

Feasibility Study of Energy Harvesting via Biofuel Cell for Miniaturised Implantable Biosensors

Supervisors

Prof. SANDRO CARRARA

Prof. PAOLO MOTTO ROS

Prof. SERAINA ANNE DUAL

Dr. GIAN LUCA BARBRUNI

Eng. ALI MEIMANDI

Candidate

REBECCA BONATO

Abstract

In the current pursuit of sustainable energy, biofuel cells are attracting considerable attention. Within biomedical engineering, the concept of harnessing energy from biological fluids, such as blood, holds significant promise, enabling both full autonomy and miniaturisation.

In this context, this study aims to identify the most efficient biofuel cells for miniaturised implantable biosensors and design a prototype based on the obtained results. To achieve this goal, a systematic literature review was conducted, comparing biofuel cells based on relevant parameters for powering devices, including power density and operative voltages. This categorisation guided material selection, considering a cost-performance trade-off. Carbon nanotubes and Laccase were chosen to facilitate oxygen reduction at the cathode. In contrast, carbon nanotubes with Glucose Oxidase (with and without ferrocenemethanol) played a similar role at the anode, where glucose proved to be the most advantageous fuel. Electrode functionalisation and assessment involved electrochemical and morphological analyses, culminating in the recording of initial results for the biofuel cell prototype.

The analysis of scientific literature revealed that under physiological conditions, including pH, glucose concentration, and single-chamber biofuel cells, the maximum power density obtained was 1 mW/cm^2 at 0.65 V. The use of nanomaterials, such as carbon nanotubes, and enzymes proved crucial for achieving this performance by enhancing electron transfer, increasing the effective area, and introducing specificity to each electrode, enabling the biofuel cell to operate without the need for a membrane. During the design phase, the functionalisation of the cathode highlighted the critical role of oxygen, which has a limited concentration in the solution. At the anode, the attempt to achieve mediated electron transfer proved successful, in contrast to the method of direct electron transfer. Finally, the characterisation of the biofuel cell demonstrated a preliminary power generation of 0.38 μW/cm^2 at 0.2 V in 500 mM glucose.

The preliminary development of the prototype confirms the feasibility of generating energy with the selected materials and highlights its limitations, laying the foundation for its optimization, such as through a more robust stabilization method. Furthermore, the project proves valuable in the context of active medical device

development, enabling a comparison between the requirements of hypothetical implantable sensors and cutting-edge technology.

keywords

Biofuel cell, Blood, Energy Harvesting, Glucose, Power density, Oxygen

Acknowledgements

Table of Contents

List of Tables

List of Figures

Acronyms

BFCs
    Biofuel Cell

OCP
    Open Circuit Potential

OV
    Operative Voltage

EBFC
    Enzymatic Biofuel Cell

MWCNT
    Multi Walled Carbon Nanotube

PBS
    Phosphate Buffer Solution

GOx
    Glucose Oxidase

DET
    Direct Electron Transfer

MET
    Mediated Electron Transfer

CV
    Cyclic Voltammetry

DPV

Differential Pulse Voltammetry

FAD

flavin adenine dinucleotide

Ag/AgCl

Silver/Silver Chloride

SEM

Scanning Electron Microscope

RE

Reference Electrode

CE

Counter Electrode

WE

Working Electrode

S

Source

Chapter 1

Introduction

Medicine is increasingly focused on the design and development of medical devices capable of effectively performing their functions while becoming less invasive for patients. In the realm of monitoring brain functions, the concept of body dust is revolutionizing the landscape as a cutting-edge alternative to conventional methods. This innovative approach could signal a transformative shift in the way we understand and implement brain function monitoring.

Body dust is intended for realizing particles that could spread in the human body floating in the vessels as thousands of individual sensors in sensing active network capable of providing telemetry from inside the body [1].
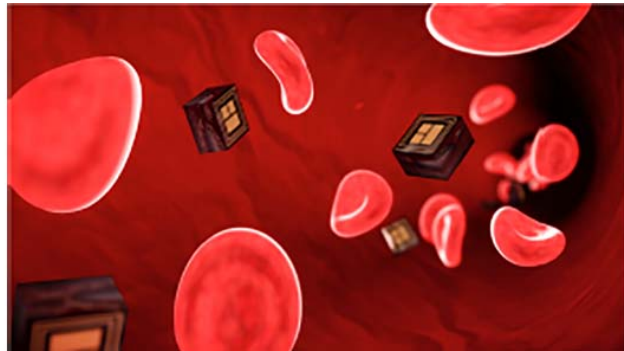
Figure 1.1: Concept of Body Dust [1].

These ultra-miniaturized devices, comparable in size to human blood cells (tens of micrometers cubes), present a formidable challenge in terms of power supply. The impossibility of incorporating conventional batteries due to their small size has prompted exploration into various wireless power transfer techniques, including inductive links, capacitive links, and acoustic links using ultrasound [2]. Despite these efforts, the limiting size of the devices hinders the efficiency

of these methods. Therefore, an alternative approach is needed, leading to the exploration of energy harvesting techniques. The term 'energy harvesting' refers to techniques aimed at capturing and converting various forms of energy available in the surrounding environment into usable energy to power electronic devices. Among these techniques, biofuel cells represent a groundbreaking advancement in bioelectronic engineering, enabling the conversion of chemicals present within the human body into a reliable source of electrical energy. It is a promising form of green energy generator that is recently growing in interest in the field of implantable medical devices such as biosensors and neurostimulators [1, 3]. Biofuel cells would make it possible to develop an implantable medical device 'self-powered' and thus independent of a battery or any form of external energy. However, the main challenges with biofuel cells are the low power density, and the long-term stability ensured during their work. Because of these outstanding challenges, the biofuel cell for biomedical applications is currently not yet used in commercialized implantable medical devices. However, several examples of working proofs of concepts can be found in the literature. For example, A. Zebda et al. [4] showed that energy collected from biofuel cell implanted in abdominal cavity of a rat produce enough energy to power a light emitting diode (LED) or a digital thermometer. Rapoport et al. [5] developed, instead, a glucose-based biofuel cells for implantable brain-machine interfaces and they demonstrated via simulation the possibility to produce 1 mW from the cerebrospinal fluid to successfully power miniaturized implant. A skin-based patch to generate energy from human sweat has been realized showing 1.2 mW/cm^2 power density under lactate physiological concentration [6].

1.1 Purpose of the project

This project aims to conduct a feasibility study of a biofuel cell as a power generator for implantable devices, paving the way for fully self-powered devices and enabling the advancement of innovative technologies such as the previously described body dust. In practical terms, this feasibility study aims:

1. to explore the most advanced technologies in the field of biofuel cells, evaluating their features and conducting a comparison among them;

2. to identify the most suitable materials for constructing a biofuel cell to power an implantable device from blood, selecting them based on a balance between cost and efficiency;

3. to implement an initial prototype of biofuel cell, highlighting key challenges and issues, and providing a foundation for the development of future optimization strategies.

2

Finally, the obtained results will be analyzed to outline the next steps regarding the optimization of the biofuel cell for implantable devices to be developed in the contest of the body dust research.

1.2 Ethics and Sustainability

The introduction of biofuel cells as power sources for medical devices, both implantable and non-implantable, responds not only to technological needs but also to the requirement for a more sustainable approach to medicine. This approach aims to promote both human health and ecological balance. Indeed, the revolutionary concept of generating energy from biological fluids like blood aligns with the realm of green and renewable energies, providing a sustainable alternative to traditional batteries or other types of power sources. Moreover, research in this field will lead to the development of increasingly stable biofuel cells capable of functioning consistently and reliably as long as the fuel is supplied, throughout the device's entire lifespan. This stands in contrast to the operation of traditional batteries, which have a significantly shorter lifespan and require replacements, posing substantial challenges for both patient health and environmental impact through increased waste generation. In light of these considerations, research in this area proves relevant to the vision of a more sustainable future and is therefore deserving of attention.

1.3 Stakeholders

The project holds fundamental significance for researchers exploring innovations in the field of biofuel cells, contributing to a broader scientific knowledge base. Future developments in the project can prove beneficial for both companies involved in the development of implantable sensor or device and patients requiring such devices for their health. A significant progress in this direction would enable companies to rely on biofuel cells as a method of powering the device, bringing substantial benefits to patients. For instance, continuous energy supply would reduce the need for surgical interventions for battery replacement and allow the creation of less invasive devices.

Chapter 2

Background

In this chapter, background information on fuel cells and their applications will be provided. Initially, the working principles will be introduced, emphasizing key factors in energy harvesting. Subsequently, the focus will shift from the broader field of fuel cells to the specific realm of biofuel cells. Within this context, a thorough analysis of blood will be conducted, exploring both its components capable of yielding energy and the challenges it poses. Following that, the types of biofuel cells, along with their characteristics and critical aspects, will be listed and explained. Finally, some of the most promising strategies employed in cutting-edge biofuel cells, particularly those designed for implantable devices, will be described.

2.1   Fuel cells

Fuel cells, also called galvanic cells, are devices designed to directly convert chemical energy into electrical energy [7]. They consist of two electrodes, the anode and cathode, that play a key role in the conversion of fuel and oxygen in the solution into electric energy through redox reactions. The electrodes are immersed in a water-based solution, serving as an electrolyte, facilitating the flow of ionic currents and containing fuels. Additionally, there is an external conductive wire that connects the cathode and anode, allowing the generated electronic current to flow between them and potentially power an interposed circuit (for instance, the electrical circuit of a medical device). Figure 2.1 provides a schematic representation of these components. Interest in the use of fuel cells as energy generators is growing due to the increasing demand for renewable energy sources [8].
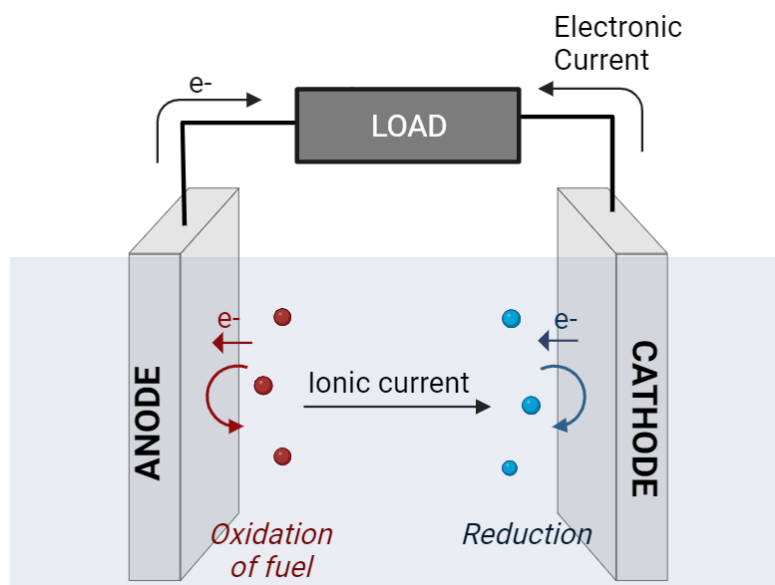
Figure 2.1: Schematic draw of a biofuel cell.

2.1.1 Working principles

Energy generation in a fuel cell is driven by redox reactions at the electrodes. Initially, the fuel undergoes oxidation at the anode, releasing electrons that are then transferred to the cathode through the external circuit. At the cathode, reduction of oxygen occurs as electrons are transferred to molecular oxygen.

The overall reaction, composed of the oxidation and reduction half-reactions at the electrodes, is spontaneous and thus characterized by a negative Gibbs free energy difference (ΔG). The Gibbs free energy is a thermodynamic state function representing the maximum free energy (i.e., the energy available to do work) that a system can exchange with the external environment during a chemical reaction at constant temperature and pressure[9]. This inherent spontaneity is the reason why this process occurs, as it signifies that the products of the redox reactions have a lower Gibbs free energy than the reactants. The change in Gibbs free energy serves as an indicator of the maximum work achievable throughout a chemical process. Consequently, there exists an inherent connection between ΔG and the standard cell's potential (E_0) described in Equation 2.1[10, 11].

$$E_0 = -\frac{\Delta G}{nF} \tag{2.1}$$

In this equation, F is the Faraday constant, and n is the number of electrons transferred in the reaction. The standard cell potential represents the maximum potential difference that can be achieved by a redox reaction under standard

conditions (i.e. a concentration of 1 M for all species involved, a pressure of 1 atm for gases, and a temperature of 25°C). Essentially, it provides a reference point for comparing the potentials of different redox reactions [12].

To calculate the standard cell potential in conditions different from the standard ones, the Nernst equation is employed 2.2.

$$E = E_0 + \frac{RT}{nF} \log \frac{[C_{ox}]}{[C_{red}]} \tag{2.2}$$

.

According to it, the theoretical cell's potential depends on the standard cell potential E_0, the gas constant R, and on environmental conditions such as temperature T, the concentration of the fuel C_{ox} and the oxygen C_{red}.

However, the theoretical potential calculated through the Nernst equation does not correspond to the actual potential physically measured between the cathode and anode in real circumstances. The efficiency of the process is limited by several types of voltage losses categorized as kinetic losses, ohmic losses, and mass-transport limitations [13]. To gain a deeper understanding of these losses, the polarization curve, depicted in Figure 2.2a in black, provides valuable insights into how cell potential changes concerning the current produced by the fuel cell [14].

In open-circuit mode, where no electronic current flows between the cathode and anode, the measured cell voltage is known as the open circuit potential (OCP), representing the maximum measurable potential for that specific cell. Whether the OCP is less than the cell potential largely depends on kinetic losses. During redox reactions, even though the products have lower Gibbs free energy than the reactants, the latter must overcome an 'activation barrier' to initiate the reaction. This activation barrier is a limiting factor that catalytic substances, such as enzymes or non-biological catalysts, can lower [14, 13, 15].

Upon closing the circuit and generating current, ohmic losses come into play. Ohmic losses follow Ohm's law and, as illustrated in Figure 2.2a, exhibit a decreasing linear trend with an angular coefficient dependent on the resistance of the electrolyte and the external circuit. Finally, for oxidation-reduction reactions to occur, reactants must reach the electrode surface. As the current increases, numerous reactions take place at the electrode, leading to the accumulation of waste products nearby [14]. Consequently, the transport of reactants to the electrode surface becomes limited. In conclusion, as depicted in Figure 2.2a, the maximum current obtained is termed the short-circuit current or limiting current. Multiplying the current values by the corresponding cell potential values provides the power generated by the fuel cell. Plotting against current or cell potential reveals at which voltage the maximum power is reached, offering crucial insights for fuel cell applications [14].

Finally it is important to mention that an essential requirement for the proper
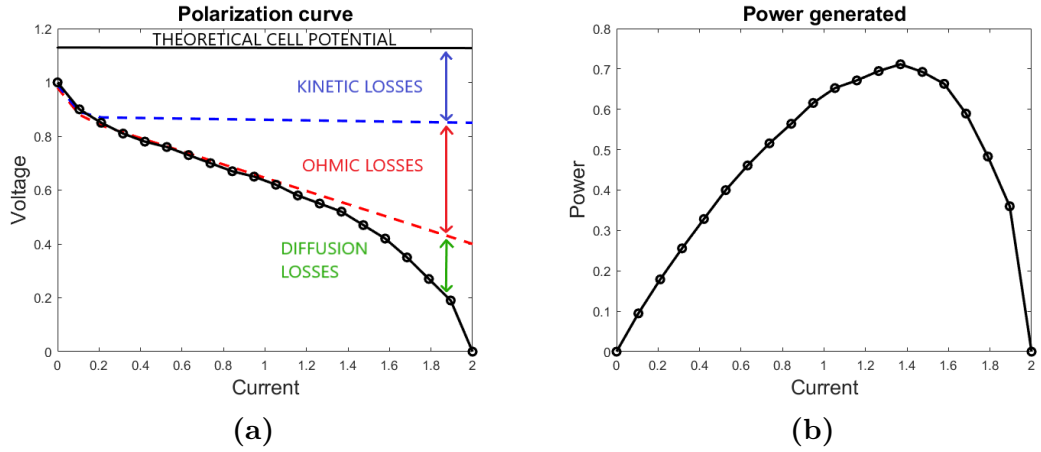
Figure 2.2: An example of polarization curve in **(a)** and the correspondent power density curve in **(b)**.

functioning of fuel cells is that the electrode potential generated at the cathode (where the reduction happens) must be higher than that generated at the anode (where the oxidation happens). This potential disparity is crucial to ensure an efficient flow of electrons through the external circuit, enabling the production of electrical current [15].

2.2   Biofuel cell

Specifically, in biofuel cells (BFCs), the solution in which the electrodes are immersed, which contains the fuel and sometimes serves as the electrolyte, is a biofluid such as blood and sweat. This configuration allows energy to be derived directly from a biofluid, paving the way for self-powering devices suitable for implantable, and wearable biomedical applications. The great advantage of using biofuel cells in biomedical applications is that they theoretically continue to function as long as the fuel contained in the biofluid is supplied [16].

A biofluid, also called biological fluid, is a fluid generated from the body. Some biofluids are naturally excreted from the body, such as urine or sweat. Others are secreted to perform specific biological functions, like breast milk or bile. Others can be obtained using a needle, such as blood or cerebrospinal fluid. Additionally, some biofluids develop as a result of pathological processes, such as those found in blister or cyst fluids [17]. Biofuel cells use a biofluid as an electrolyte, which must contain the compound to be oxidized at the anode and the compound to be reduced at the cathode for it to function properly. In particular, implantable devices use blood as the biofluid through which the biofuel cell must produce energy.

2.2.1 Harvesting energy from blood

Blood is a body fluid with multiple vital functions such as conveying oxygen and essential nutrients to the body tissues, forming clots to prevent excessive bleeding, regulating body temperature, transporting antibodies and other immune system cells, conveying waste products to the kidneys and liver for purification of the blood, etc [18]. Blood is composed of plasma and formed elements. Plasma is the liquid component of blood, it consists of 90% of water and it serves as a vehicle for the corpuscular elements. Its crucial role involves transporting nutrients and waste throughout the body. Various compounds, including proteins, electrolytes, carbohydrates, minerals, and fats, are dissolved. The formed elements consist of cells and cell fragments suspended in the plasma. The three classes of formed elements encompass erythrocytes (i.e. red blood cells), leukocytes (i.e. white blood cells), and thrombocytes (i.e. platelets) [19].

To derive energy from an electrochemical cell, it is necessary to have blood components capable of undergoing reduction (i.e. acquiring electrons) and oxidation (i.e. releasing electrons) processes. Regarding the oxidation process, key blood constituents dissolved in plasma, suitable for this purpose, are presented in Table 2.1 along with their physiological concentrations in human blood.

Table 2.1: Blood compounds.

BLOOD FUELS	
COMPOUND	CONCENTRATION
GLUCOSE	3,9-5,9 Mm [20]
LACTATE	0,3-1,3 mM at rest [21]
UREA	1,8 - 7 mM [22]
FRUCTOSE	8,1 µM [23]
KETONE BODIES	50 µM (traditional diet) [24]
OXYGEN	0,02-0,06 mM [25]

Glucose is a simple sugar, present in the blood in the form of D-glucose. It plays a fundamental role as a source of energy for the body's cells, since it undergoes oxidation through a series of enzymatic reactions to release energy. The initial step of this process involves the enzymatic action of glucose oxidase, which catalyzes the oxidation of glucose. The reaction is as follows:

$$\beta - D - glucose \rightarrow \delta - gluconolactone + 2H^+ + 2e^- \tag{2.3}$$

Essentially, glucose is transformed into gluconolactone, and during this conversion, two protons and two electrons are released. The released electrons are crucial carriers of energy and can be exploited in electrochemical cells to generate electrical energy.

Lactic acid is an organic compound generated from the anaerobic metabolism of glucose, specifically through the reduction of pyruvate at the end of glycolysis. Lactic acid tends to then dissociate into an anion, called lactate, and a proton. The lactate present in the blood can undergo an oxidation reaction where two electrons are released, as highlighted in Equation 2.4 [21].

$$Lactate \rightarrow pyruvate + 2H^+ + 2e^- \tag{2.4}$$
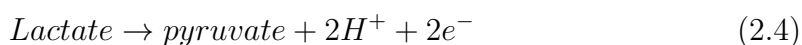
Fructose is a simple sugar that can undergo oxidation, primarily metabolized in the liver, and consequently present in smaller quantities in the blood. Urea, a nitrogen-containing chemical compound, is a byproduct of protein metabolism and is primarily excreted through urine. While urea is capable of undergoing oxidation processes, this biochemical transformation in the bloodstream, at physiological pH, is intricate. Consequently, there is currently no documented literature on biofuel cells using urea in the blood for energy generation. Notably, extensive exploration has been directed toward the production of energy utilizing urea found in urine [8].

Ketone bodies, vital for brain energy during fasting, are produced in the liver through fat metabolism. Acetoacetate (AcAc) and 3-beta-hydroxybutyrate (3HB) are the principal ketone bodies, with acetone being the least prevalent. Their concentrations in blood are typically maintained at low levels [26, 24].

As evident from the considerations just made, lactate and glucose are typically employed as fuels for both implantable and wearable biofuel cells. The selection of these fuels is driven by their concentrations in the order of millimoles (mM) and the relatively straightforward oxidation processes they undergo.

We now turn our attention to the analysis of oxygen, which undergoes reduction as indicated by Equation 2.5.

$$O_2 + 4H^+ + 4e^- \rightarrow 2H_2O \tag{2.5}$$

Oxygen is conveyed within the bloodstream through two mechanisms: dissolution in plasma and the water content of red blood cells, constituting approximately 2% of the total, and reversible binding to hemoglobin, accounting for approximately 98% of the total. It is essential to underscore that only the dissolved oxygen in plasma, determined by Henry's law, is pertinent to the reduction process in the biofuel cell, with a concentration ranging from 0.02 to 0.06 mM. In addition to the

challenge posed by the low oxygen concentration in solution, it is noteworthy that the diffusion rate of oxygen in aqueous solutions is considerably slow [27].

It is important to note that, referring to biofuel cells involved in generating energy from blood, we are talking about those known as single-chamber fuel cells. In other words, the fuel and oxygen are contained in the same fluid, and therefore, the electrodes must be capable of operating under mixed conditions (i.e., in the presence of both oxygen and fuel).

Furthermore, it is crucial to consider that, in contrast to serum which is composed of 90% of water, the presence of blood cells and various interferents in human blood adds an extra layer of complexity for implantable biofuel cells [28]. Indeed, molecules such as ascorbic acid, dopamine, and others pose a dual challenge. On one hand, due to their volumetric hindrance, they limit the access of fuel and oxygen to the active sites on the electrode, reducing the efficiency of redox reactions and electron transfer. On the other hand, the interaction of these molecules with the electrodes could lead to undesired chemical reactions, limiting the long-term stability of the system[28].

Finally, it is relevant to specify that the pH of the blood is 7.35-7.45 while its temperature is about 37°C. These are all conditions to be taken into account when replicating the in vitro functioning of a biofuel cell.

2.3   Types of biofuel cells and electron transfer

A crucial point for the functioning of biofuel cells is the redox reactions at the electrode. The complete oxidation-reduction reaction is spontaneous (i.e. the free energy of the products is less than the free energy of the reactants); however, a certain activation energy must be exceeded for the reaction to take place. The role of a catalyst is to decrease the activation energy without changing the overall reaction mechanism and thus without affecting the characteristic Gibbs free energy of the reactants and products as it is shown in Figure 2.3. Moreover, at the end of the reaction, the catalysts are not consumed and consequently do not become part of the products and are ready to catalyze the reaction again. The lower the activation energy that the reactants have to overcome, the faster the reaction[29, 30]. Depending on how the catalysis takes place, fuel cells can be subdivided into abiotic, enzymatic, and microbial. Another aspect of fundamental importance to biofuel cell operation is electron transfer. As the name implies, it refers to the process whereby electrons are transferred at the end of oxidation from the biofuel to the anode and from the cathode to the oxygen for reduction to take place. This process differs depending on the type of biofuel cell being considered and is often a major challenge for energy conversion efficiency [31].
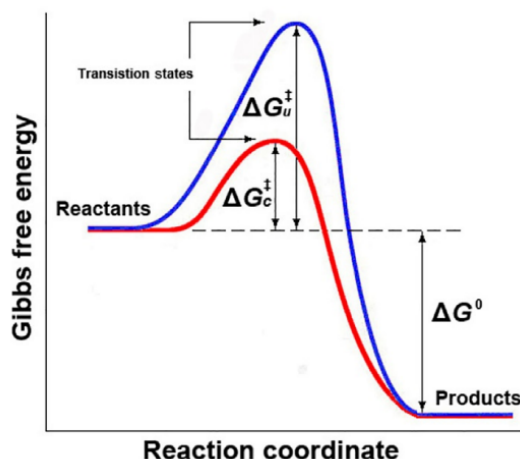
Figure 2.3: Catalyst role in a spontaneous reaction. In blue is shown the Gibbs activation energy path when a catalyst is not used; in red, the Gibbs activation energy path when a catalyst is used [29].

2.3.1 Microbial Biofuel Cells

Microbial catalysis is a process in which microorganisms play a key role in facilitating chemical reactions, particularly in the realm of biofuel cells. In microbial catalysis within biofuel cells, a microorganism acts as a bioreactor at the anode, promoting the oxidation of substrates such as glucose. Simultaneously, at the cathode, an abiotic catalyst facilitates the reduction of oxygen (Figure 2.4). This approach harnesses the natural abilities of microorganisms, allowing them to operate in typical environmental conditions without the need for the extraction and purification of enzymes. The microorganism operates within its usual environmental conditions, and one of its notable strengths is the ability to perform multiple oxidation steps. An distinctive aspect of microbial catalysis is the ability of microorganisms to undergo multiple oxidation steps, enabling a significant release of electrons. For instance, during the complete oxidation of glucose at the anode, a high number of electrons per glucose molecule can be released. This characteristic distinguishes microbial catalysis from other approaches, such as enzymatic biofuel cells, which are often limited to a single oxidation step[16, 32].

However, a critical factor is to maintain conditions appropriate to the life of the microorganism. Factors like temperature, pH levels, and the availability of nutrients play a vital role in ensuring the microorganism's health and optimal performance when integrated into the biofuel cell system [34]. Despite the extensive research and development in the field of microbial biofuel cells, achieving efficient energy conversion remains a formidable challenge due to the intricate nature of the
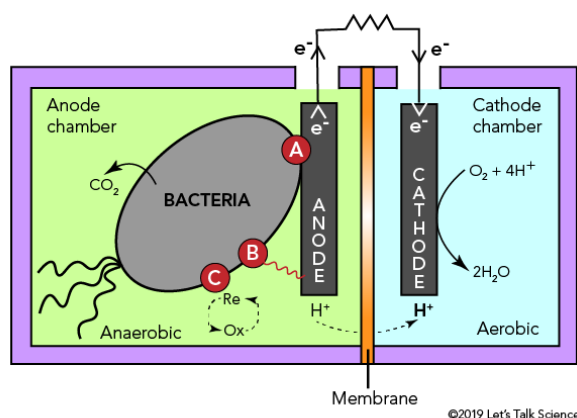
Figure 2.4: Example of a microbial biofuel cell [33].

underlying biochemical processes [34].

2.3.2 Enzymatic Biofuel Cells

Enzymatic biofuel cells (EBFC) represent a unique category within the realm of biofuel cells that leverage biological enzymes as electrode catalysts. One of their most notable features is the remarkable specificity of these biocatalysts, effectively mitigating the occurrence of undesired cross-reactions in a membrane-less biofuel cell [35].

As it is shown in Figure 2.5, each enzyme plays a dual role: an active center that serves the purpose of selectively detecting the target molecule and a redox center that acts as an electron acceptor when the target molecule is oxidized.
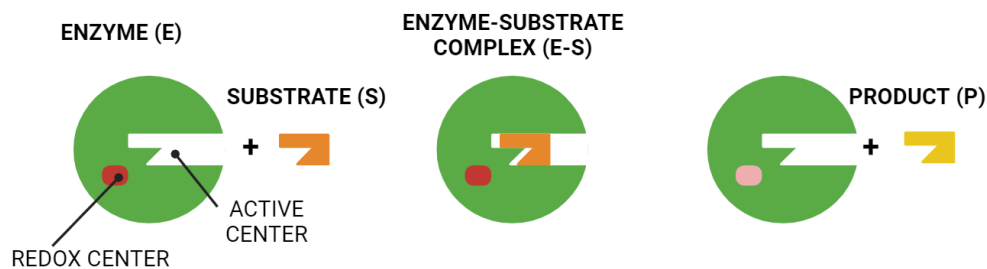
Figure 2.5: Enzyme structure: activation and redox center.

However, it's important to specify that the operation of the enzyme immobilized on the electrode of a biofuel cell is slightly different from what occurs when the enzyme is free in solution. In fact, the electrode needs to substitute for one of

12

the enzyme's half-reactions in its natural setting. In other words, the electrode should serve as the ultimate electron acceptor or donor, depending on whether it's operating as a bioanode or biocathode, respectively [31]. For this to occur, electrons must undergo a process called direct electron transfer (DET), where they are transferred directly from the enzyme's redox site to the electrode, without the involvement of any other species in the transfer. However, it has been demonstrated that efficient direct transfer occurs only when the path traversed by electrons is less than 2nm [36, 3, 31].

Another mechanism of electrons transfer relies on the incorporation of redox mediators during the construction of the bio-electrode, known as mediated electron transfer (MET). In summary, an additional step takes place: the fuel undergoes oxidation at the redox center within the enzyme; the enzyme's redox center becomes oxidized, transferring electrons to the mediator, which in turn becomes reduced; finally, the mediator undergoes oxidation at the electrode, transferring the electrons. The primary aim of employing mediators is to enhance the electron transfer rate between the redox-active site of the biocatalyst and the electrode [37]. The choice of the mediator must adhere to certain constraints. Specifically, at the anode, the mediator's potential must be greater than that of the enzyme's cofactor, and conversely at the cathode [31].
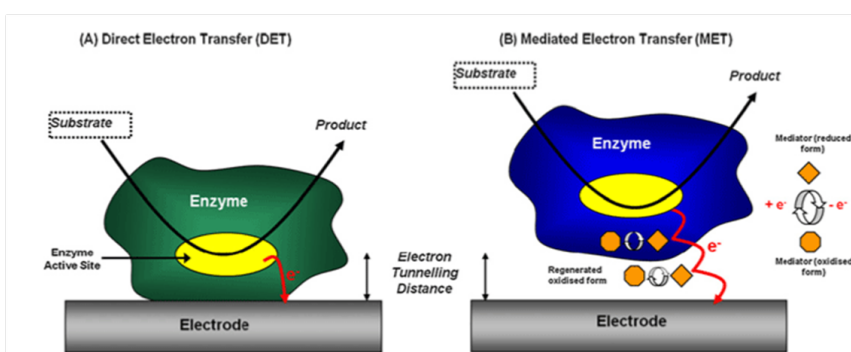
Figure 2.6: Direct and mediated electron transfer mechanism [38].

However, the presence of a mediator introduces certain drawbacks. The immobilization of a mediator frequently requires complex procedures and leads to a reduction in the theoretical OCP of the biofuel cell, determined by the potential difference between the prosthetic sites of the two enzyme types involved. Additionally, the potential leakage of the mediator from the electrode can impact long-term performance and may give rise to potential toxic concerns [39], particularly in the context of implanted biofuel cells [40].

When mentioning enzymatic biofuel cells, it is appropriate to briefly refer to enzymatic kinetics, which is one of the elements regulating the reaction rate and,

consequently, one of the factors influencing the amount of generated current. At the core of this kinetics lies the Michaelis-Menten law (Equation 2.6), explaining the relationship between the rate of an enzymatic reaction and the concentration of the substrate.

$$V = \frac{V_{max}[S]}{K_M + [S]} \tag{2.6}$$

It suggests that the rate V increases with rising substrate concentration $[S]$ but reaches saturation when all enzymes are fully engaged. The K_M constant provides a measure of the enzyme's affinity for the substrate [41]. Visually, this relationship can be easily understood by observing Figure 2.7.

$$E + S \underset{k_{-1}}{\overset{k_1}{\rightleftharpoons}} ES \xrightarrow{k_2} E + P$$
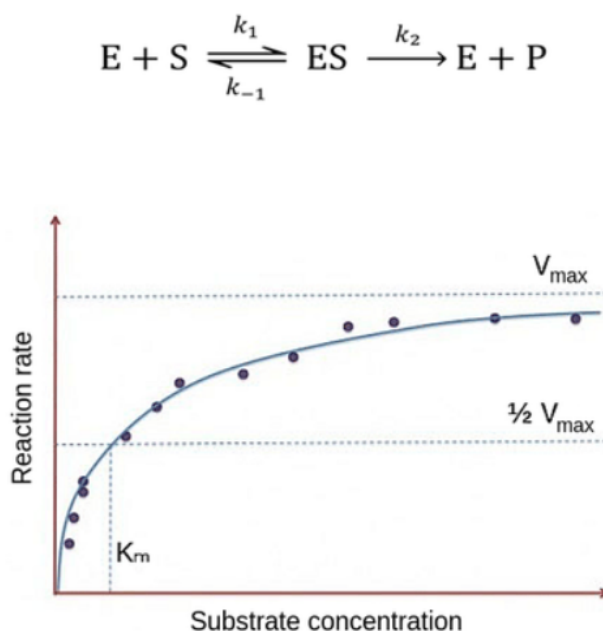
Figure 2.7: Michaelis Menten law [42].

2.3.3 Abiotic Biofuel Cells

Abiotic biofuel cell exploits non-biological catalysts for the oxidation of biological species. Their implementation is relatively straightforward compared to enzymatic and microbial biofuel cells. However, a significant challenge lies in achieving a high degree of specificity in the catalytic activity. The low specificity means that potentially at the same electrode, both fuel oxidation and oxygen reduction can take place. If this happens, the device is unable to function as a biofuel cell

and consequently fails to generate the desired voltage and current. To avoid this problem, the ideal would be to use a membrane to divide the anodic and cathodic compartments and ensure that the anodic compartment contains exclusively the biofuel while the cathodic compartment is exposed to air and contains oxygen [34].

When faced with the challenge of difficult separation between the anodic and cathodic electrolytes, alternative solutions come into play as shown in Figure 2.8. Drawing inspiration from biological catalysts, efforts have been made to create abiotic catalysts characterized by heightened selectivity for glucose oxidation and oxygen reduction reactions. The objective is to achieve comparable selectivity and activity, surmounting the stability and charge transfer impediments associated with enzymatic catalysts. This involves a realm of materials science, exploring noble metals, carbon, ceramics, and their combinations [25].

Another viable approach is the adoption of a design strategy known as the depletion design. This method entails isolating one electrode from direct contact with the fuel-containing liquid. A selective catalyst at the fuel-facing electrode depletes one species, leading to a diminished concentration of that species at the other electrode. This design effectively creates an oxygen-free fuel at the anode side of the fuel cell. However, challenges arise from the slow diffusion of reactants and products to and from the buried electrode, resulting in high overpotential and decreased power output [25]. A notable application of this design strategy is exemplified by Rapoport et al.[5] in the development of a biofuel cell for brain-machine interface applications.

Perm-selective membranes provide another solution by allowing the selective passage of only one reactant to an electrode surface, creating a two-chamber fuel cell configuration. These membranes, placed at one or both electrodes, block one species from reaching the electrode while allowing the other to pass through. This design approach eliminates the necessity for selective catalysts, enabling the utilization of highly active yet non-selective catalysts like platinum [25].
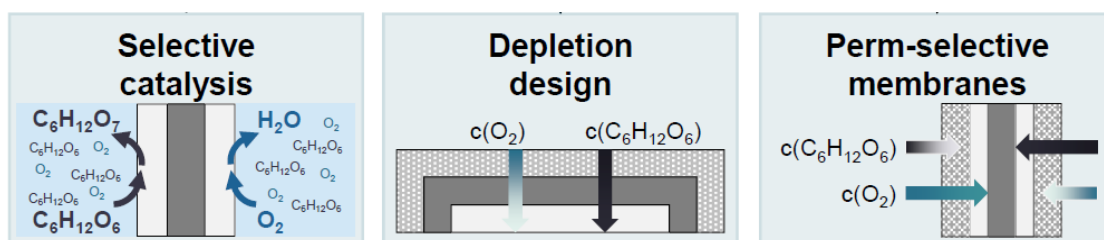
Figure 2.8: Strategies to be selective in the abiotic catalysis [25].

2.4   State of the art

As for implantable biofuel cells, historical attempts have been made in various animal subjects. For instance, the first biofuel cell was implanted in 2010 in the retroperitoneal space of a freely moving rat, generating a power output of 2 µW [43]. Subsequent attempts involved implantation in a cockroack [44], a snail [45], and two live lobsters connected in series [46]. In the latter case, it was even possible to power a digital watch. To approach closer to the human organism, numerous experiments have been conducted in rats. For example, in a study conducted by A.Zebda et al.[4], a biofuel cell was implanted in the retroperitoneal cavity of a rat, producing a power output of 38.7 µW at 0.57 V. Subsequently, a miniaturized biofuel cell was introduced into the jugular vein of a rat, generating 95 µW at a potential of 80 mV for approximately 24 hours [47, 3].

On the other hand, given the difficulty in obtaining authorization for in vivo testing of biofuel cells, numerous biofuel cells have been tested in vitro, achieving significant performances. The most high-performing biofuel cells developed so far have been organized in Table A.1 shown in the appendix.
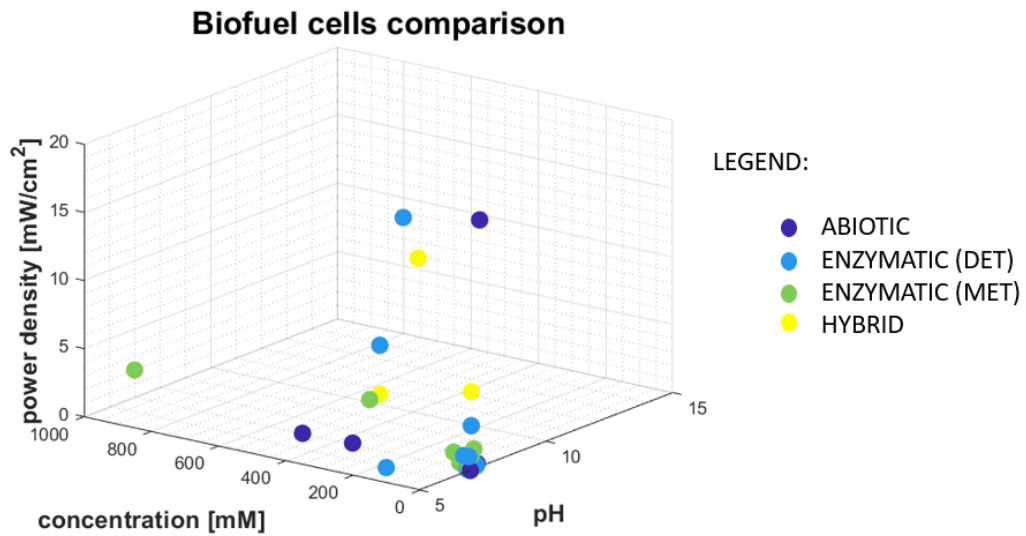
Figure 2.9: Comparison of biofuel cell with respect pH, concentration of fuel and power density.

If we visualize these biofuel cells with respect to pH, fuel concentration, and generated power density, as shown in the figure 2.9, it becomes evident that testing conditions for constructed biofuel cells vary significantly. This variation poses challenges when attempting to make meaningful performance comparisons.

The graph presented in Figure 2.10 narrows down the field to biofuel cells tested under conditions of pH and fuel that align more closely with physiological parameters.
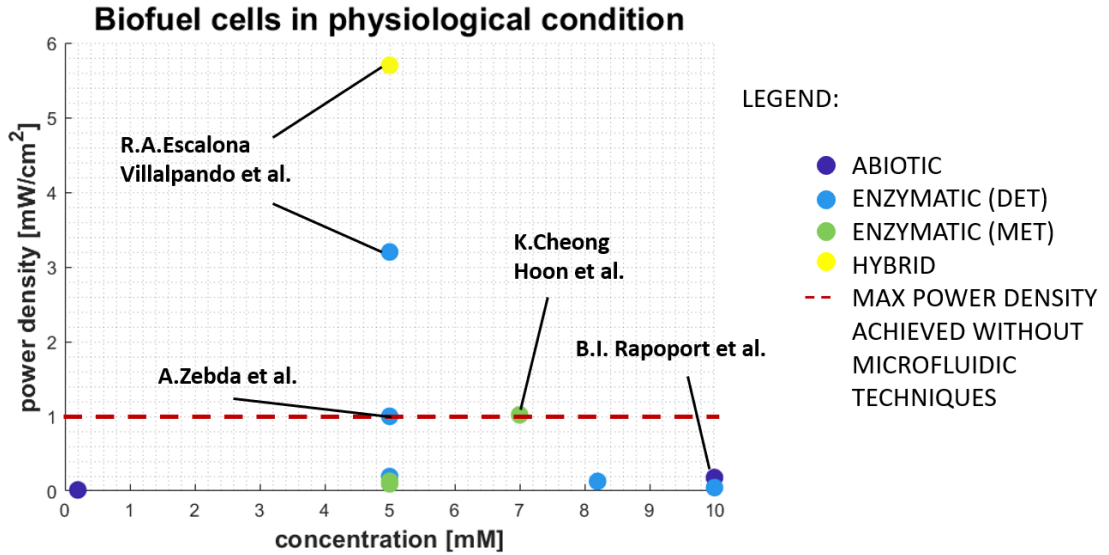
Figure 2.10: Biofuel cells at physiological pH and concentration.

As a consequence of this operation, the achievable maximum power drops dramatically, highlighting how the concentration of glucose influences the performances, as one would expect. Furthermore, pH also has its effects: aside from abiotic biofuel cells, which in some cases demonstrate significantly higher performances at basic pH, oxygen reduction enzymes such as Bilirubin Oxidase and Laccase also work optimally at a pH around 5, diminishing their performances when the pH reaches physiological levels.

Going into details, Figure 2.10 shows that the higher performances achieved in terms of power density, despite utilizing a low concentration of glucose (5mM), are 5.7 mW/cm^2 and 3.2 mW/cm^2. Both of these biofuel cells, as shown in Figure 2.11c, were developed by R.A.Escalona Villalpando et al. [48] using a microfluidic system with separate anodic and cathodic chambers, a configuration challenging for implantable devices where glucose and oxygen are mixed. The fabrication method for the latter involves immersing sheets of carbon nanofoam in a solution of glutaraldehyde (used as a crosslinker) and either Laccase or Glucose Oxidase. By substituting the cathode with a spray-coated Pt electrode, the performances increase, reaching the power density mentioned before of 5.7 mW/cm^2

In contrast, biofuel cell technologies developed under conditions more aligned with current implantable devices have demonstrated a maximum power output of 1 mW/cm^2 [40]. In this work A. Zebda et al. created carbon nanotube discs

through mechanical compression, incorporating enzymes for glucose oxidation and subsequent direct electron transfer (Glucose Oxidase) at the anode, and for oxygen reduction (Laccase) at the cathode. Additionally, Catalase enzyme is incorporated at the anode to decompose hydrogen peroxide, which accumulates near the electrode during the glucose oxidation reaction as an undesired effect. The effective use of nanomaterials in this manner has allowed for efficient direct electron transfer, resulting in a power density of 1 mW/cm^2 at a potential of 0.65 V in a solution composed of 5mM glucose. Long-term stability in this case is also ensured by a cellulose membrane that wraps each disc, preventing the diffusion of enzymes into the solution [40]. A schematic of the biofuel cell is shown in Figure 2.11a.

A similar power density equal to 1.02 mW/cm^2 is shown by the biofuel cell built by K.Cheong Hoon et al. [49]. The authors developed robust and flexible MWCNT fibers by coating them with PEDOT polymer, a process generated through biscrolling. The fundamental concept of biscrolling involves coating a sheet of carbon nanotubes with the desired enzyme, followed by twisting and weaving the resulting stack to create a thread or fabric. The efficiency of this technique stems from its capability to deposit substantial amounts of the enzyme within the carbon nanotubes, maintaining high electrical conductivity, mechanical strength, and flexibility in the resultant material. The enzymes employed in this study are Glucose Oxidase at the anode and Bilirubin Oxidase at the cathode. However, mediators are utilized to facilitate efficient electron transfers at both the anode and cathode, following the MET mechanism. The system has been tested in human serum with a concentration of glucose equal to 7 mM and it is shown in Figure 2.11b. In addition, it is important to mention that both described biofuel cells utilize carbon nanotubes at the electrodes to mediate electron transfer. It is also interesting to note that, within the investigated concentration range, only the two biofuel cells mentioned achieve performances of such magnitude. After them, there is a gap where numerous other applications reach a power not exceeding 200/300 µW.

The biofuel cells described so far were all enzymatic or hybrid. Instead, concerning abiotic biofuel cells, it's worth mentioning the work by B.I. Rapoport et al., which exemplifies the so-called "depletion design." In this setup, the cathode is made up of a mesh of carbon nanotubes completely covering the platinum nanostructure anode. Additionally, a Nafion membrane is placed between them. This design creates an oxygen gradient that significantly improves oxygen reduction at the cathode as depicted in Figure 2.11d. Glucose reaches the protected anode by diffusing through the nanotube mesh and the Nafion layer, which allows the passage of small neutral and cationic particles. The power produced in a steady state is 3.4 µ W/cm^2 [5].

Furthermore, it is also interesting to mention some innovative strategies, still in the study phase, aimed at maximizing the quantity of electrons obtained from the

(a) *A. Zebda et al.[40].*

(b) *K. Cheong Hoon et al [49].*

(c) Microfluidic based biofuel cell [48].

(d) *B.I. Rapoport et al.* [5].
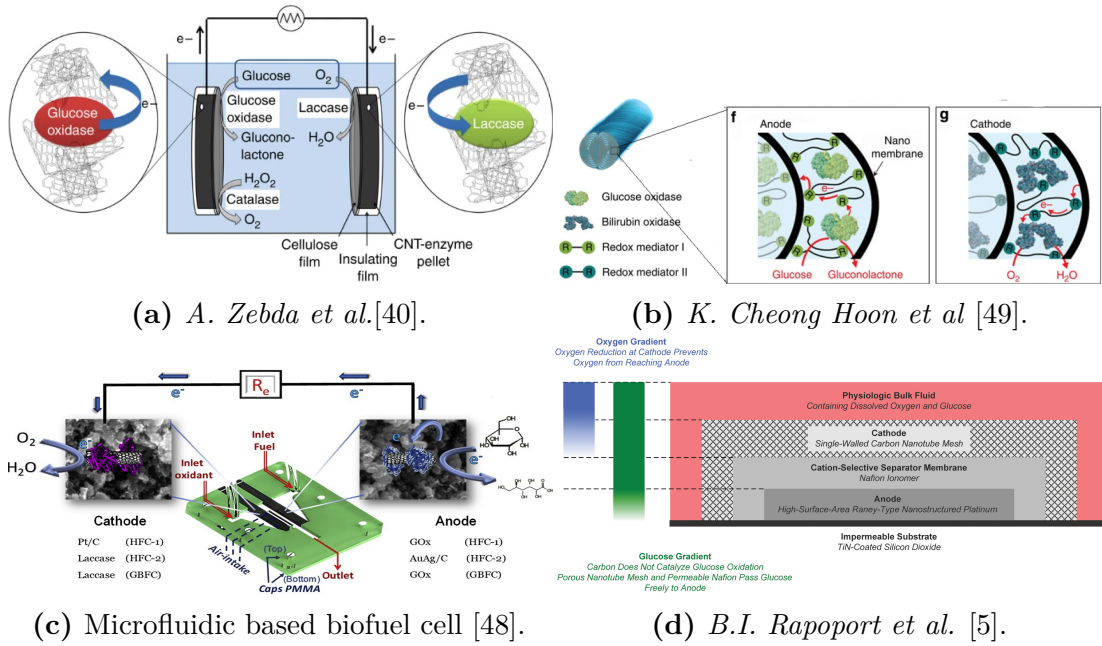
Figure 2.11: Most interesting biofuel cell from the State of the Art.

oxidation process and transferring them to the electrode.

In the biofuel cell developed by I. Shitanda et al. [50], instead of utilizing only one step of lactate oxidation to pyruvate and gaining two electrons from the oxidation process through lactate, the incorporation of Pyruvate Oxidase as a second enzyme at the anode allows for the subsequent oxidation of pyruvate obtained in cascade from lactate. This is a way to doubly exploit lactate: at the same lactate concentration, obtain a greater number of electrons.

Finally, another strategy is to create a multisugar biofuel cell capable of being selective towards multiple types of fuels at the anode, not just a single one, to enhance performance. This has been achieved by Y. Chen et al. through an abiotic biofuel cell, requiring a membrane to function, with the anode based on Co_3O_4. Given the significant catalytic capabilities of this nanomaterial, glucose, sucrose, and lactose can be simultaneously used for energy production [51]. Although this strategy cannot be directly applied as developed in the context of implantable devices, as it involves having the cathode and anode in two separate chambers, it can provide an interesting insight into the direction in which biofuel cells are moving to extract as much energy as possible.

Chapter 3

Materials and Methods

In this chapter, the methodology employed in the exploration and development of a biofuel cell will be elucidated. The first step involves a systematic analysis of biofuel cells found in the literature to highlight the power density values that can be expected. This analysis plays a pivotal role in guiding the material selection for the prototype's implementation. Subsequent sections will outline the methodology for both implementing and evaluating the biofuel cell prototype. The initial focus will be on the individual electrode components—the anode and cathode. Following that, attention will be redirected towards the overall construction and evaluation of the BFC entirely.

3.1 Choices for implementation of a biofuel cell for implantable sensors

The objective of this section is to outline the methodology employed for conducting a systematic analysis of biofuel cells designed for implantable devices. Additionally, this section aims to describe the methodology involved in selecting the type of biofuel cell to be implemented and choosing the corresponding materials for prototype development

3.1.1 Analysis of cutting edge technology in biofuel cell

One of the biggest challenges in analyzing biofuel cells realized so far is to compare them. This is a critically important step in choosing the materials with which to make the prototype, among the purposes of this thesis. To solve this problem, the investigated biofuel cells have been systematically organized in Table A.1 (detailed in the Appendix), emphasizing the following enumerated parameters with explanations justifying their inclusion:

1. **Generated Power Density:** Extracting this parameter is crucial for evaluating the maximum power that the biofuel cell can supply to the device to be powered. In the Table A.1, only biofuel cells from the literature with a power density of at least 1 µW/cm² have been included, unless they are interesting from other perspectives.

2. **Operating Voltage (OV):** Although not always explicitly reported, this parameter can be deduced from the power density curve. Its significance lies in the fact that a device must be designed to operate at a well-defined voltage, not exclusively at a specified power level.

3. **Type of Fuel and Solution:** Reporting the type of fuel used, along with its concentration in the solution, is crucial for ensuring a correct comparison and verifying which options have been tested under physiological conditions.

4. **Operating Conditions (pH and Temperature):** pH and temperature play a significant role in influencing the generated power performance. Including these operating conditions provides context and aids in understanding the biofuel cell's behavior under specific environmental factors.

5. **Electrode Material**: the material of the electrodes is reported to offer insights into manufacturing details and assess biocompatibility. While not a current criterion for selection, future considerations, being an implantable device, may involve evaluating electrode materials for biocompatibility.

6. **Type of Biofuel Cell:** categorizing biofuel cells based on types (e.g., abiotic, enzymatic with direct electron transfer, enzymatic with mediated electron transfer) provides insights into prevalent approaches and their respective advantages.

7. **Application or Purpose:** Reporting the intended application or purpose of the biofuel cell provides a broader context, aiding in understanding the specific scenarios for which these cells were designed.

It would have been interesting to report the size of the electrodes made. Unfortunately, this parameter is not easy to deduce: sometimes it is not provided, and sometimes the size of the biofuel cell is specified without mentioning the electrodes.

To allow for a more intuitive visualization, a 3D graph has also been created in which each biofuel cell is represented concerning the pH at which it operates, the fuel concentration that is used to achieve the maximum performance mentioned in the corresponding paper, and the power per unit area generated under these conditions (Figure 2.9). In the same figure, abiotic biofuel cells, enzymatic cells

functioning by direct electron transfer (DET), enzymatic cells based on mediated electron transfer (MET), and hybrid cells (in which one between anode and cathode is abiotic and one is enzymatic) are indicated with different colors.

Implantable devices impose stringent requirements for these parameters, particularly demanding physiological glucose concentration and neutral pH. Notably, there is no identified standard procedure for reporting biofuel cell performances measured with high glucose concentration or non-physiological pH, corresponding to the standard measure. Consequently, biofuel cells not meeting these criteria are excluded from the subsequent comparison shown in Figure 2.10. In particular, the representation is restricted to biofuel cells operating at pH equal to 7 and a fuel concentration of less than 10 mM.

3.1.2 Material's choice

As mentioned above, biofuel cells can be microbial, enzymatic, or abiotic. To decide which of these was more ideally suited to implantable devices, the advantages and disadvantages of each were summarised. The scientific literature and the state of the art were consulted to derive the comparison. It is important to note that microbial biofuel cells have been excluded from this investigation, with the subsequent discussion focusing on enzymatic and abiotic biofuel cells. The exclusion is motivated by the fact that microorganisms used in microbial biofuel cells are predominantly bacteria, which could pose health risks when implanted in the human body. This option has been ruled out since the focus here is on implantable devices. However, studies propose using stem cells as microorganisms in microbial biofuel cells, such as employing neuronal-like cells to build a single-chamber biofuel cell, as seen in A. Belkis et al.[52]. While promising, this area is still in its early stages of research and development. On the other hand, the realm of abiotic and enzymatic biofuel cells has been more explored, with richer scientific literature on the subject. They have their own set of pros and cons that are interesting to analyze in the context of implants.

Indeed, when it comes to selectivity, implanted devices must be selective towards the fuel at the anode and towards oxygen at the cathode. This is particularly important since oxygen and glucose (or any other fuel that may be used) are not separated from each other. If this does not happen, there could be reduced oxygen at the anode and oxidized fuel at the cathode, leading to a short circuit in the biofuel cell. As mentioned earlier in chapter 2, the role of enzymes is to enhance selectivity. On the other hand, paying price for increasing the complexity of the design, the same goal can be achieved through abiotic means by complicating the design and increasing the size.

From the perspective of power density, the analysis suggests that enzymatic-based biofuel cells are capable of producing higher power values at neutral pH.

Table 3.1: Comparison between biofuel cells' type and body dust requirements.

	REQUIREMENTS IMPLANTABLE DEVICES	ABIOTIC	ENZYMATIC
SELECTIVTY	Selectivity towards fuels at anode and oxygen at cathode	Low selectivity	Enzyme's role increases selectivity
POWER DENSITY	1 µW at pH = 7 and body temperature	Better performances at basic or acidic pH	Perform better at neutral pH
STABILITY	It depends on the specific application	High stability	Lifetime of enzymes needs to be taken into account
FABRICATION PROCESS	/	Stable	The stabilization of enzymes and mediators on the electrode is challenging

However, enzymatic activity is not unlimited, unlike abiotic biofuel cells, which are certainly more stable. The main problems that can arise when enzymes come into play include the detachment of enzymes (and any mediator) from the electrode, as well as the loss of enzymatic activity. Despite this drawback, this comparison, presented in Table 3.1, helps guide the choice towards an enzymatic-type biofuel cell.

For the choice of material with which to fabricate or functionalize the electrode, the surface characteristics of the materials were identified as having a high impact on the performance of the biofuel cell. The state of the art was taken into account as well as price, material availability, and the feasibility of the procedure. These considerations shaped the methodology employed in the selection process.

The selected commercial screen-printed electrode, employed as a substrate for both anode and cathode functionalization, is the Dropsense 11L from Metrohm. It is characterized by a 4mm diameter carbon working electrode, a carbon counter electrode, and a Silver/Silver chloride (Ag/AgCl) reference electrode as shown in Figure 3.1.
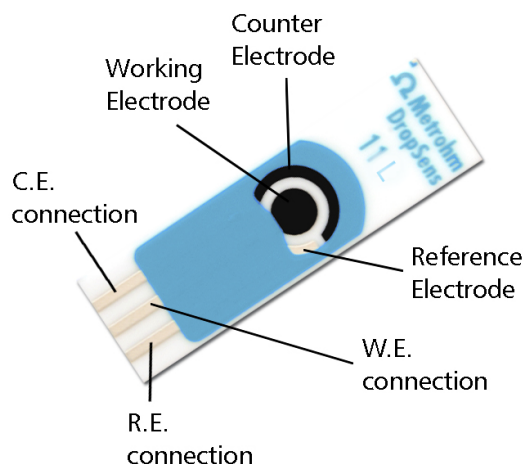
Figure 3.1: Commercial screen printed electrode.

Concerning the anode, the enzyme Glucose Oxidase (GOx) isolated from Aspergillus niger has been selected because it is the essential enzyme for glucose electrochemical sensing and is considered the gold standard. It is characterized by high specificity for glucose [53]. However, due to the buried FAD (flavin adenine dinucleotide) redox cofactor within the protein, direct electron transfer to the electrode is not efficient (Figure 3.2a). Nevertheless, numerous biofuel cells operate through direct electron transfer using electrodes fabrication involving nanomaterials such as carbon nanotubes. This is the case, for example, in R.A. Escalona-Villalpando et al. [48] and A. Zebda et al. [40], among the most high-performing ones analyzed.

At the cathode, on the other hand, the enzyme Laccase has been chosen, which, together with Bilirubin Oxidase, represents the most commonly used enzymes for such applications. Both of these enzymes belong to the family of multicopper oxidases and are characterized by having 4 copper centers in the protein structure: through them, the process that converts the final electron acceptor, O_2, into H_2O_2 occurs [54] (Figure 3.2b). The electron transfer is reported to be easier compared to the glucose oxidase case.

One challenge in employing enzymes as catalysts in biofuel cells is ensuring effective electron transfer between the enzyme and the electrode surface. One approach to address this issue involves utilizing various nanostructures, such as carbon nanotubes, fullerenes, graphene derivatives, and gold nanoparticles [58]. These nanostructures play a pivotal role in reducing the distance electrons need to travel from the enzyme's redox center to the electrode surface, facilitating a process not noteworthy if this distance is more than 2 nm. The nanostructures selected are multi-walled carbon nanotubes (MWCNTs). Indeed, they are characterized by a high surface area-to-volume ratio. In the context of sensing or biofuel cells, this
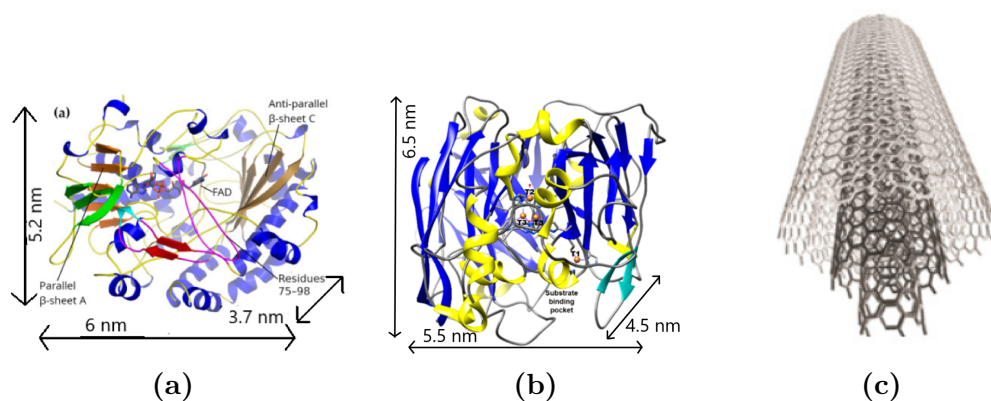
Figure 3.2: (a): glucose oxidase from Aspergillus niger [55]. **(b)**: Laccase from Trametes versicolor [56]. **(c)**: MWCNTs [57].

feature is crucial as it allows for an increased surface area necessary for enzyme stabilization, resulting in a significantly larger effective area than the geometric area (Figure 3.2c). Furthermore, their structure makes them particularly conducive to enzyme immobilization, finding a favorable support for their stabilization [57]. On the other side, the use of nanomaterials, particularly MWCNTs, is accompanied by a drawback related to their toxicity[59]. The choice of carbon nanotubes has also been guided by the advantageous trade-off between cost and utility, particularly favorable compared to other nanomaterials. Finally, ferrocenemethanol has also been purchased with for role of a further mediator to facilitate mediated electron transfer at the anode.

3.2 Electrodes functionalization and assessment

In this section, the methods employed for the functionalization and evaluation of a chosen commercial screen-printed electrode are delineated. Functionalization refers to the deposition of material on top of the electrode for various purposes such as increasing conductivity and specificity.

At each step of the electrode functionalization process, the quality and homogeneity of the material deposition were analyzed and evaluated. To commence, an electrochemical assessment of the functionalized electrode was conducted using an Autolab potentiostat/galvanostat electrochemical workstation from Metrohm (PGSTAT101). The experimental setup for electrochemical analysis remained consistent throughout the entire process and will be described here, with subsequent sections referring to this configuration. The setup for measurement acquisition is depicted in Figure 3.3. The functionalized screen-printed commercial electrode was immersed in a beaker containing a pH 7 buffer solution with varying concentrations
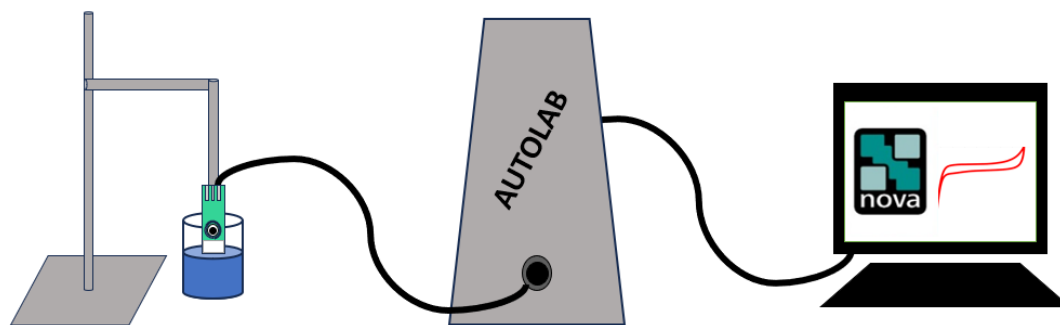
Figure 3.3: Electrochemical measurement setup.

of glucose, secured in place by a metal holder. The working, reference, and counter electrodes were connected to the Autolab hardware, which, in turn, was linked to a personal computer running the Nova 2.1 software. Through the interface of this software, measurements could be acquired.

The techniques used for data collection are two: cyclic voltammetry and differential pulse voltammetry.

The second analysis performed on the surface of the functionalized electrodes is morphological. First of all, such an analysis makes it possible to analyze qualitatively whether the functionalization steps of the electrode took place as expected (e.g. nanotubes visible on the electrode surface, enzyme deposition changes the morphology of the nanotubes,etc). The second objective of this analysis is to visually assess the homogeneity of the functionalization of the electrode. For the application of biofuel cells in which the generated power is evaluated in terms of power per unit area of the electrode, it is crucial to ensure that each part of the electrode contributes approximately equally to power generation. The result of this analysis is intended to guide the optimization of the electrode functionalization process to obtain better results in electrochemical analysis. A scanning electron microscope (SEM) is chosen to perform the morphological analysis due to the high resolution allowed by the instrument. The samples are conductive and therefore the analysis can be conducted without the addition of another conductive layer on the sample.

3.2.1 Cyclic voltammetry

Cyclic Voltammetry (CV) is an electrochemical technique that measures the current generated by cyclically varying the potential of a working electrode, providing insights into redox reactions occurring on the electrode surface[60]. A graphical representation can be observed in Figure 3.4. This library is available on Autolab Metrohm under the name *Cyclic Voltammetry Potentiostatic.*
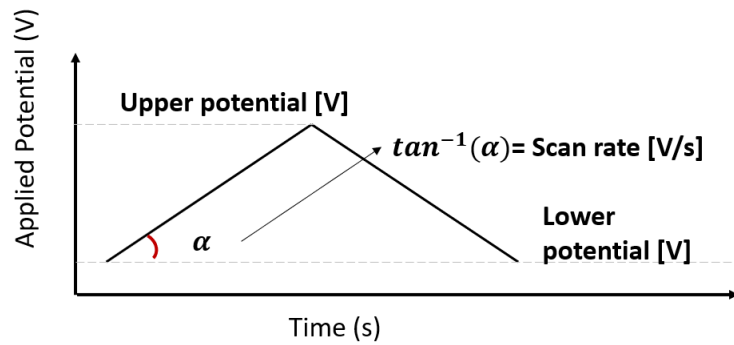
Figure 3.4: Cyclic voltammetry for anode characterization.

3.2.2 Differential Pulse Voltammetry

Differential pulse voltammetry is a technique in which pulses of constant amplitude are applied on a linear ramp potential as it is shown in Figure 3.5. Current is
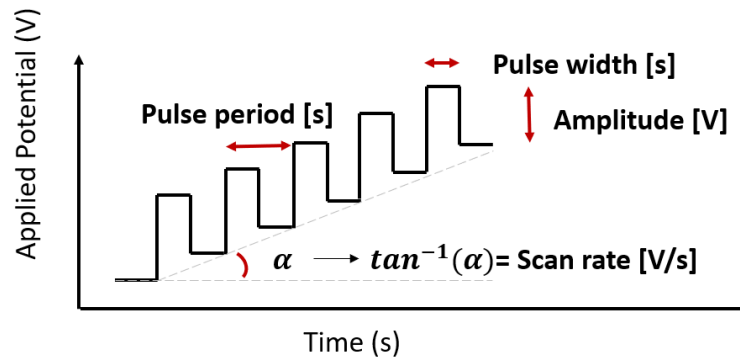
Figure 3.5: Differential pulse voltammetry for cathode characterization.

recorded both before and after the pulse application and the difference between them (called δ current) is recorded [61]. The advantage of this technique over cyclic voltammetry is its greater sensitivity due to the minimization of capacitive currents. Furthermore, all effects that remain constant before and after the pulse application are not visualized, thanks to the subtraction of currents performed[61]. To record data using this technique, the custom library *Cyclic Voltammetry Potentiostatic* was selected in Autolab, and the *Cyclic Voltammetry* block was replaced with the *Differential Pulse* block.

27

3.2.3 Baseline subtraction

Baseline subtraction is a data analysis procedure aimed at eliminating a consistent background signal from experimental electrochemical data. To achieve this, two points are identified—one before and one after the peak under examination. These points are interpolated using a polynomial curve that captures the trend of the electrochemical signal in the absence of the peak to be isolated and analyzed.

In subsequent experiments, a straight line is employed for interpolation. At this point, the peak is subtracted from the identified polynomial curve as it is shown in Figure 3.6. The baseline subtraction procedure has been implemented using a MATLAB code.
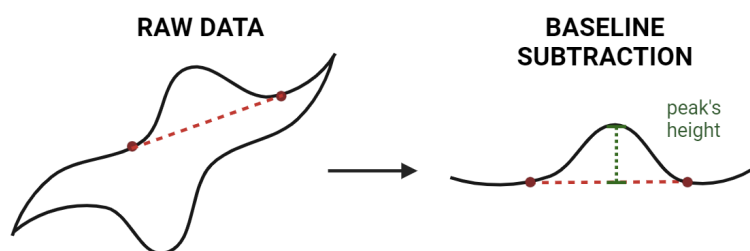
Figure 3.6: Baseline subtraction.

3.2.4 Multi-Walled-Carbon-Nanotubes

The initial functionalization of both the anode and cathode involves drop-casting MWCNTs onto a commercial screen-printed electrode (Metrohm, Dropsense 11 L). The primary objective is to investigate the morphological and electrochemical effects resulting from this deposition.

For this study, COOH-functionalized MWCNTs obtained from Metrohm are prepared and dropcasted using the following procedure. MWCNTs are dissolved in 2 mL of chloroform (Sigma Aldrich) to achieve various concentrations: 0.1 mg/mL, 0.3 mg/mL, 0.5 mg/mL, 0.7 mg/mL, and 0.9 mg/mL. Chloroform is selected as the solvent for MWCNTs due to its excellent solubility and chemical compatibility with organic compounds. Its effectiveness in dissolving MWCNTs ensures a uniform dispersion and facilitates manipulation during experiments.

To address the issue of carbon nanotubes to form aggregates, sonication is employed for approximately 40 minutes. This process ensures an even dispersion in the solution and disrupts any aggregates formed, thanks to the application of ultrasound waves [62].

Subsequently, the solution is deposited onto the screen-printed electrode using a micropipette in drops of 3 µL each. The dropcasting in multiple steps is necessary

due to the spreading nature of chloroform. During the procedure, MWCNTs tend to reaggregate. A viable solution involved employing vortexing to thoroughly mix the solution, thereby enhancing control over the homogeneity of MWCNTs in a more precise manner. The total amount of solution deposited is 30 µL. For each concentration of MWCNTs, three electrodes were functionalized.

The electrochemical analysis was performed using cyclic voltammetry with the functionalized electrode immersed in a phosphate-buffered saline (PBS) solution. The parameters set are a lower voltage of -0.6 V, an upper voltage of 1 V, a scan rate of 100mV/s and the number of scans performed are 4. The first scan is discarded, while the subsequent three scans are utilized to calculate the charge storage capacity, according to the following formula:

$$\frac{1}{S * \nu} \int_{E_1}^{E_2} I(E) \, dE \tag{3.1}$$

where S is the geometrical area of the electrode $[cm^2]$,ν is the scan rate [V/s], I is the current [A] while E_1 and E_2 are the cutoff potential [V][63]. Taking into account the parameters just mentioned, the charge storage capacity has been chosen as a parameter to identify the overall changes made to the electrode following functionalization. The results are reported as the mean value across three electrodes, accompanied by the standard deviation.

3.2.5 Cathode

Cathode functionalization involves the sequential drop-casting of MWCNTs in chloroform and Laccase from Trametes versicolor, obtained from Sigma Aldrich. The preparation and drop-casting of MWCNTs follow the procedure described in subsection 3.2.4, using a 1 mg/mL concentration of MWCNTs in chloroform. Subsequently, Laccase is dissolved in PBS (pH = 7) to achieve a concentration of 15 mg/mL. The solution is gently mixed, and 10 µL are deposited on the electrode in a single step. The functionalized electrode is then left to dry at 4°C overnight.

From an electrochemical perspective, the electrodes underwent analysis through differential pulse voltammetry (DPV) using the experimental setup mentioned earlier (Figure 3.3), as depicted in Figure 3.5. A similar measurement was performed on an electrode functionalized solely with MWCNTs for comparison. The parameters utilized for the analysis are summarized in Table 3.2. The selection of cutoff potentials was made because the literature suggests the expectation of observing a peak within this range, attributed to the presence of laccase [40, 64]. Three measurements were taken for each electrode, and the results are presented in terms of standard deviation and mean value on the same electrode. The data were also subjected to baseline subtraction to enhance the identification of peaks. Subsequently, a morphological analysis was conducted through SEM.

Table 3.2: Differential pulse voltammetry for cathode analysis.

Cathode analysis	
PARAMETER	VALUE
Upper potential	0.8 V
Lower potential	0.2 V
Pulse period	0.2 s
Pulse width	0.05 s
Amplitude	0.05 V
Scan rate	10 mV/s

3.2.6   Anode: direct electron transfer method

As for the anode functionalization, two methods exploiting enzymatic catalysis were investigated. Initially, a systematic approach was taken to establish a functional anode via direct electron transfer. Subsequently, through the introduction of a mediator, exploration was conducted to achieve mediated electron transfer.

The first procedure involves the sequential deposition of MWCNTs and glucose oxidase through dropcasting. A chloroform solution of MWCNTs, with a concentration of 1 mg/mL, is prepared and dropcasted according to the procedure outlined in subsection 3.2.4. Subsequently, Glucose Oxidase from Aspergillus niger (purchased from Sigma Aldrich) is dissolved in PBS to achieve various concentrations: 2 mg/mL, 5 mg/mL, 8 mg/mL, and 12 mg/mL. Each solution is gently stirred to facilitate mixing and is then deposited onto the surface of the MWCNTs in 10 µL aliquots. Due to the highly hydrophobic nature of MWCNTs, this deposition can be conducted in a single step. The electrodes prepared in this manner are stored in the refrigerator at approximately 4 °C overnight to allow for enzyme adsorption.

After preparing the electrodes, with three samples for each concentration along with an additional one without Glucose Oxidase deposited, various electrochemical analyses are conducted. Initially, utilizing the same setup in Figure 3.3, cyclic voltammetry is performed in PBS at different scan rates, both for electrodes functionalized with glucose oxidase and those functionalized solely with MWCNTs. The potential range from -1 V to +1 V is chosen to align with the carbon's water window, ensuring that electrochemical processes occur in a controlled and safe manner, avoiding water decomposition. This approach is adopted due to the exploratory nature of the analysis, aiming to comprehensively assess any alterations resulting from the functionalization process with glucose oxidase in PBS.

Subsequently, the analysis involves studying cyclic voltammetry when glucose is introduced into the PBS solution. Accordingly, glucose solutions in PBS are prepared at various concentrations (0.5 mM, 1 mM, 2 mM, 3 mM, 4 mM) following Equation 3.2

$$C_{glucose}[M] = \frac{m[g]}{V_{solvent}(L) * M[\frac{g}{mol}]} \tag{3.2}$$

where $C_{glucose}$ is the desired glucose concentration, m is the mass of the added glucose, $V_{solvent}$ is the volume of the solvent and M is the molecular weight of glucose.

The cyclic voltammetry measurements are conducted in glucose solutions prepared as described above, with an upper potential set to 1 and a lower potential set to -1. The scan rate used is 20 mV/s. Furthermore, the current peaks identified in cyclic voltammetry were analyzed in terms of baseline subtraction to verify whether an increase in peak height occurs with the escalating glucose concentrations, as expected in the enzymatic detection zone. Data analysis is conducted as follows:

1. Identification of peaks through baseline subtraction for each cyclic voltammetry and each electrode at the pre-defined glucose concentrations.

2. The maximum value for each peak is then identified: the intra-electrode mean and standard deviation of this value are calculated for each glucose concentration. Using these values, a regression line and the corresponding coefficient of determination are calculated. The choice to interpolate with a line is made under the assumption of being in the linear zone of enzymatic detection. The coefficient of determination indicates how well the line interpolates the derived points.

3. The slope of the regression line, indicative of the sensitivity of enzymatic detection, is calculated.

The obtained results are reported in the corresponding results section without inter-electrode variability. This is because not all electrodes at the end of the experiment proved functional due to errors in functionalization (e.g., enzyme solution migrating onto the counter electrode during absorption on MWCNTs, causing measurement discrepancies).

3.2.7 Anode: mediated electron transfer method

The transition from attempting to achieve direct electron transfer to mediated electron transfer is executed by directly introducing the chosen mediator (Ferrocenemethanol purchased from Sigma Aldrich) into a solution in which cyclic

voltammetry is conducted. The objective of this analysis is to verify the activity of the mediator. The procedure consists into adding 5 mg of ferrocenemethanol into each previously prepared glucose solution. Using electrodes on which a concentration of 8 mg/mL of Glucose Oxidase has been deposited, cyclic voltammetry is performed with a scan rate of 20 mV/s. In this case, as well, the results are analyzed in terms of baseline subtraction, a calibration curve is constructed, and sensitivity is calculated.

Finally, the subsequent procedure involves the deposition of the mediator on the electrode. Specifically, a solution of 1 mg/mL MWCNTs in chloroform is prepared and deposited on the electrode as previously described. As a second step, ferrocenemethanol is dissolved in PBS at different concentrations (0.25 mg/mL, 0.5 mg/mL, 0.75 mg/mL, and 1 mg/mL) and deposited onto the initial coating of MWCNTs in a volume of 10 µL. The mediator is allowed to dry for a few hours in a fume hood. Finally, 10 µL of Glucose Oxidase at a concentration of 8 mg/mL (prepared as explained earlier) is in turn deposited on the electrode. The electrodes are stored overnight at 4°C. The electrochemical analysis was conducted through cyclic voltammetry, employing a voltage range between -1 V and 1 V with a scan rate of 20 mV/s, baseline subtraction, and oxidation and reduction peaks identification.

3.3   Biofuel cell characterization

In this section, the methodology for constructing a biofuel cell by coupling the cathode and anode, along with its characterization, will be outlined.

The setup used for measurements is described in Figure 3.7. Autolab galvanostat/potentiostat (Metrohm) is employed as the measuring tool in the so called two-electrode configuration. In this setup, the cable labeled reference electrode (RE) and the one labeled counter electrode (CE) are connected and linked to the cathode. Conversely, the working electrode (WE) and the sense(S) are connected to the anode. The two electrodes are immersed in a solution of pure PBS, a solution containing 5mM of glucose, and a solution containing 500 mM of glucose. The electrodes are supported by a metal holder to maintain a constant distance between them (about 0.5 cm) during the measurement.

In parallel with the potentiostat and the circuit formed by the two electrodes and the electrolyte, different resistors are sequentially connected: 2.72 Mohm, 0.819 Mohm, 0.286 Kohm, and 26.9 Kohm. Additionally, measurement is conducted without connecting any resistor in parallel: the so-called open circuit potential measurement. The Autolab library named *open circuit potential* is used to perform this measurement. The potential generated by the coupling of the two electrodes is
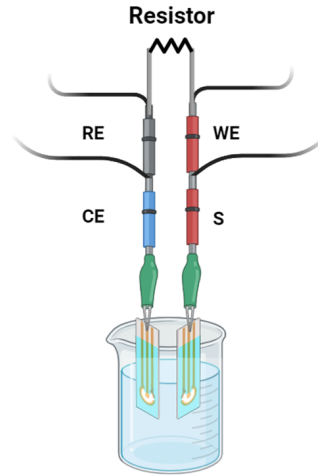
Figure 3.7: Biofuel cell setup.

recorded for 5 minutes for each configuration to allow stabilization. A 5 s moving average is applied to the signal during acquisition to obtain a more stable measurement. The voltage value obtained after 5 minutes is considered for subsequent data analysis.

The subsequent data analysis involves the calculation of the power density curve and the polarization curve, which are useful for biofuel cell characterization. For each previously obtained voltage, the power density is calculated according to the relationship:

$$P = \frac{V^2}{RA} \tag{3.3}$$

where R is the resistor employed for the measurement and A the geometric area of the working electrode. Then, the current density, useful for determining the polarization curve, is calculated according to Ohm's law.

The procedure described above is tested for two electrode configurations, as indicated in Table 3.3.

Table 3.3: Biofuel cell testing: anode and cathode coupling.

		Anode	Cathode
1.	MWCNTs and GOx	MWCNTs+Laccase
2.	MWCNTs and ferrocenemethanol and GOx	MWCN + Laccase

Chapter 4

Results and Discussion

In this chapter, the results and discussion concerning the implementation of the biofuel cell prototype according with the material and method chosen are presented. Specifically, the experimental results related to the cathode, along with relevant considerations, will be reported first. Subsequently, the outcomes of experiments conducted on the anode will be analyzed: initially regarding the direct electron transfer method and then about the mediated electron transfer. Finally, the outcomes that come from building the biofuel cell are showcased, emphasizing how well it performs in terms of power density output and voltage.

4.1 Electrodes functionalization

In this section results related to the functionalization of the electrode are reported. In particular, first, the effect of the deposition of carbon nanotubes on the electrode surface will be shown both electrochemically and morphologically, compared with the bare electrode. Then, the same electrochemical and morphological evaluations carried out on the enzyme-modified electrode will be reported. The concept of focusing on the characterization of the anode and cathode separately before proceeding to the complete biofuel cell stems from the goal of not only constructing a functional biofuel cell but also identifying its primary issues or performance limitations. This approach aims to pave the way for the design of a customized optimization process.

4.1.1 Multi-Walled-Carbon-Nanotubes dropcasting

Considering that both the anode and cathode have undergone functionalization with Multi-Walled Carbon Nanotubes as the initial step, this section is dedicated to a comprehensive analysis of the MWCNTs functionalization process, examining

both the electrochemical and morphological aspects. Figure 4.1 illustrates the trend in charge storage capacity as the concentration of deposited MWCNTs on the electrode varies, comparing it with the bare electrode.
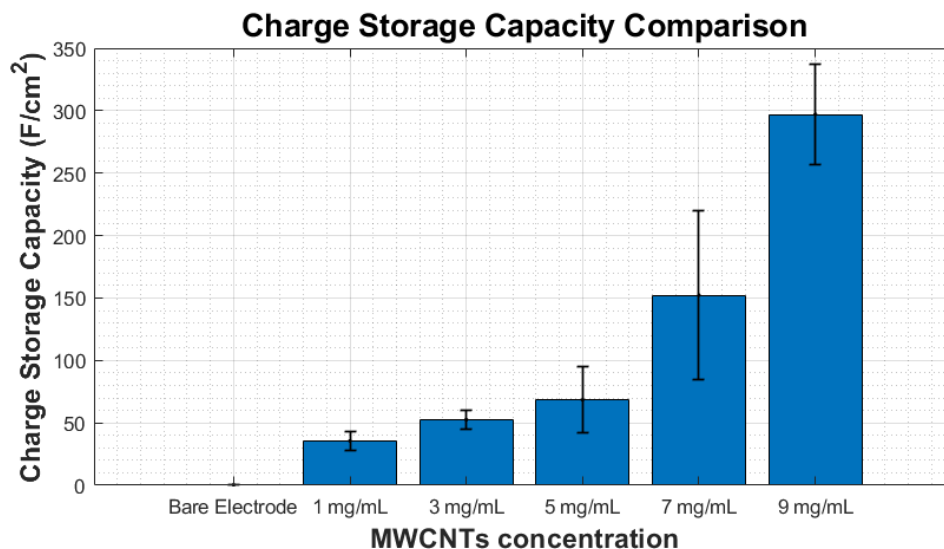
Figure 4.1: Charge storage capacity adding 30 microL of MWCNTs in different concentration on bare electrode surface.

The estimation of this parameter, as outlined in Formula 3.1, relies on factors such as the area beneath the cyclic voltammetry curve, the geometric area of the electrode, and the scan rate. Given the constancy of the latter two parameters, the substantial variation in the average value primarily pertains to the first parameter—the area of the CV. This parameter is indicative of the quantity of charge exchanged during the observed electrochemical process. It is crucial to highlight the observed growth in the area under the CV concerning the increasing concentration of MWCNTs.

Notably, the difference in charge storage capacity between the bare electrode and a concentration of 9 mg/mL is approximately two orders of magnitude. Furthermore, attention should be drawn to the escalating standard deviation as the quantity of deposited MWCNTs increases. This phenomenon can be attributed to the better dispersion of the MWCNTs and chloroform solution at lower concentrations. Conversely, at higher concentrations, the risk of depositing clumps or areas with poorer dispersion rises, introducing variability. This variability stems from the inherent instability of the solution at elevated concentrations.

From a morphological standpoint, the results of the SEM scans of the electrodes are depicted in the following figures. Specifically, in Figures 4.2a and 4.2b a portion of the bare electrode is observable at different scales (2 µm and 200 nm), while in Figures 4.3a and 4.3b, the same is done with the electrode functionalized with

MWCNTs.

(a) Scale: 2 µm.

(b) Scale: 200nm.
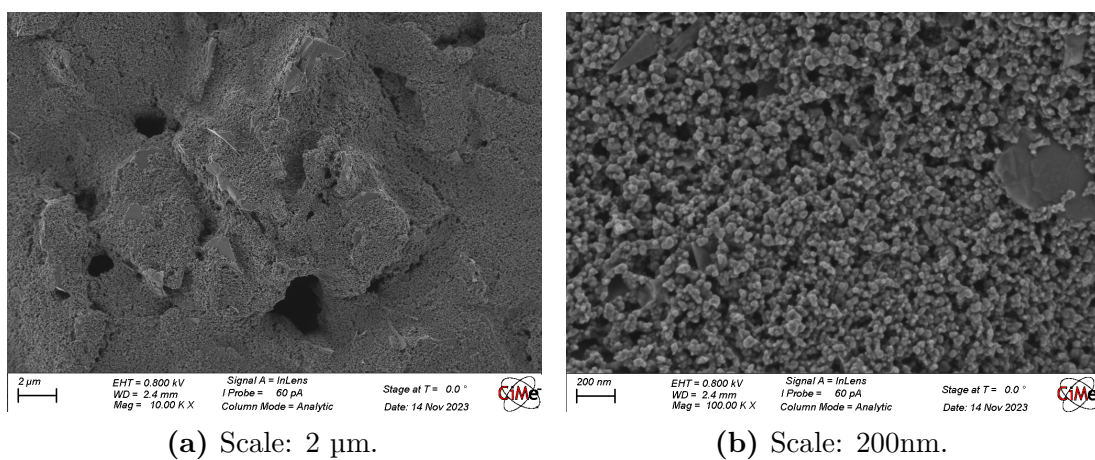
Figure 4.2: SEM pictures of Bare Electrode

(a) Scale: 2 µm.

(b) Scale: 200nm.
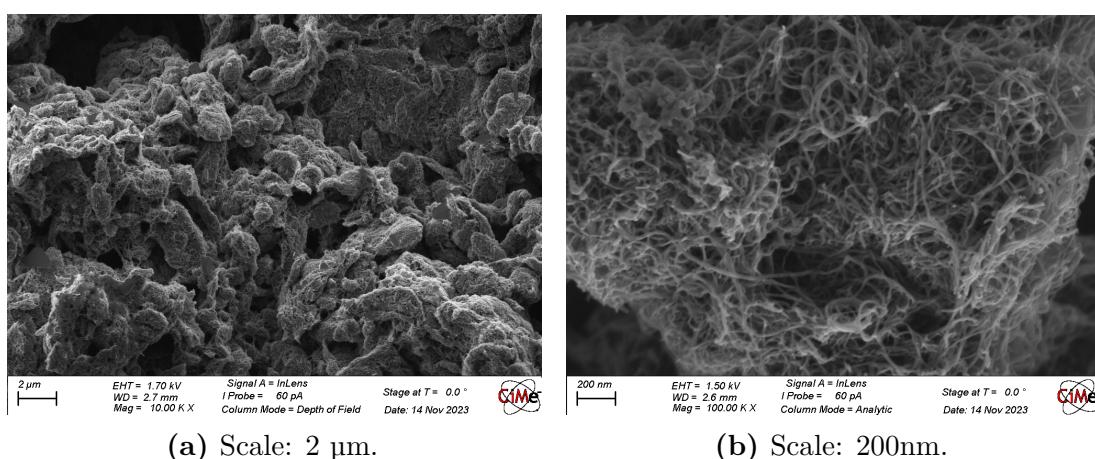
Figure 4.3: SEM pictures of MWCNTs deposited on the electrode.

From the mentioned pictures is possible to morphologically appreciate the surface modification induced by MWCNTs, which introduces an increase in the effective area of the electrode. Indeed, the volumetric surface no longer appears on a single plane but takes on a three-dimensional configuration, as visible in the comparison between Figures 4.2a, showing the bare electrode at the scale of 2 µm and Figures 4.3a where the electrode functionalized with MWCNTs is shown at the same scale. In applications such as electrochemical sensing and biofuel cells, the three-dimensional area of the electrode is a critical factor. This factor becomes especially significant as it directly influences the enzyme attachment and catalytic

processes. A larger three-dimensional area provides more space for enzymes to anchor, leading to increased catalytic efficiency.

Furthermore, in Figure 4.3b at a smaller scale (200 nm), the actual shape assumed by the MWCNTs is observable, and their diameter can be estimated. Calculated from 20 well-defined nanotubes in the figure, the average diameter is found to be 19.57 nm. At this scale, the augmentation of the available surface area for enzyme attachment becomes even more pronounced.

Finally, it is important to highlight that the SEM microscope also reveals the limitations of the dropcasting method. The surface deposition of MWCNTs is non-uniform, tending to be higher at the edges and in the center of the electrode. This aspect introduces variability in the results of functionalization.

Given the importance of MWCNTs in enhancing the sensitivity of electrochemical glucose and oxygen detection, the potential impact of non-uniformity on the performance of a biofuel cell should not be underestimated. In fact, if certain portions of the electrode are not sufficiently functionalized with MWCNTs, they will have a diminished impact on electron current generation. Similarly, clusters of MWCNTs impede the electron transfer, as the charge tends to accumulate rather than flow toward the electrode. To maximize efficiency, it is crucial to optimize the process deposition further.

4.1.2   Cathode functionalisation

The following subsection deals with the outcomes and discussion of cathode functionalization. Assessing its effectiveness, particularly in mediating the reduction of oxygen, allowing direct electron transfer and evaluating its proper deposition on the electrode, is pivotal and has been thoroughly examined through conducted characterizations.

The electrochemical analysis involves evaluating the results of the differential pulse voltammetry (DPV) in PBS for an electrode functionalized solely with MWCNTs (depicted in blue) and an electrode functionalized with both MWCNTs and Laccase (depicted in red). The Figure 4.4a illustrates these outcomes as the potential varies from 0.2 V to 0.8 V (direct differential pulse voltammetry). Conversely, in Figure 4.4b, the potential varies from 0.8 V to 0.2 V (inverse differential pulse voltammetry). The graph presents the results in terms of mean values and standard deviations derived from measurements conducted on the same electrode.

A distinct contrast is observable when Laccase is deposited on MWCNTs compared to the scenario where only MWCNTs are deposited. Although peaks are subtly discernible, there is a noticeable difference, accentuated by the larger standard deviation in the case of Laccase deposition. However, through subsequent baseline subtraction analysis, the distinction between the two curves becomes more
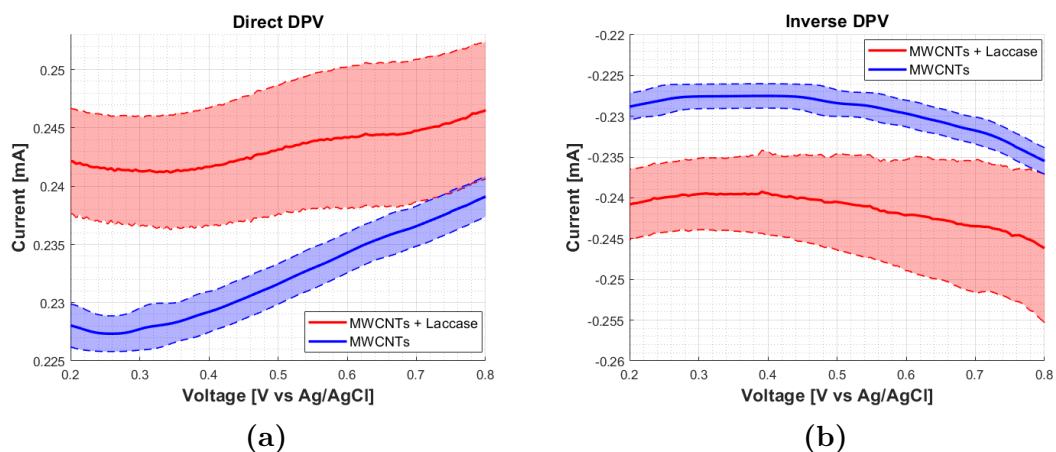
Figure 4.4: (a): Direct differential pulse voltammetry. **(b)**: Inverse differential pulse voltammetry.

pronounced.
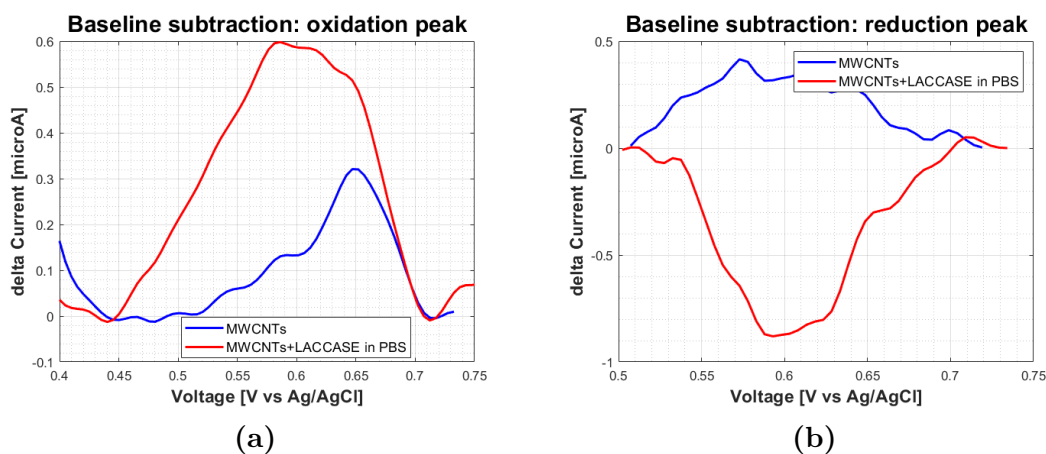
Figure 4.5: (a): Oxidation peak after baseline subtraction. **(b)**: Reduction peak after baseline subtraction.

Regarding the oxidation peak shown in Figure 4.5a, it is evident that even in the absence of Laccase deposition, a peak is present. However, this peak intensifies when Laccase is introduced onto the MWCNTs. Conversely, concerning the inverse differential pulse voltammetry aiming to identify the reduction peak, the difference is more substantial as observable in Figure 4.5b. Specifically, the curve in the case of only MWCNTs appears concave, whereas in the case of functionalization with Laccase, the reduction peak is evident.

Several considerations merit attention. Firstly, these results suggest effective

Laccase functionalization on the electrode, as evidenced by the peak falling within the range identified in the literature as appropriate for the electrochemical activity of Laccase. However, varying the oxygen concentration in the solution to observe changes in the peak could offer additional insights. This would ensure proper electron transfer and confirm that the detected peak doesn't solely reflect the electrochemical behavior of the enzyme Laccase. This can be achieved by saturating the solution with Nitrogen to reduce oxygen and analyzing whether the corresponding peak decreases.

This process is significant because enzymes with a redox center exhibit inherent electrochemical activity independent of the substrate, in this case, oxygen.

Additionally, it's crucial to note that differential pulse voltammetry, designed for enhanced resolution in detecting electrochemical peaks, isn't directly comparable to results obtained through cyclic voltammetry. While this technique can highlight peaks not easily discernible in cyclic voltammetry, the observed peak in our analyses is relatively modest (1 µA for the reduction peak). On one hand, this peak could potentially be enhanced through further optimization of Laccase deposition. On the other hand, it underscores a significant challenge: the concentration of dissolved oxygen in the solution is limited, representing a system constraint that should not be disregarded. However, an approach to potentially enhance the efficiency of direct electron transfer is to explore deposition techniques for Laccase that promote an orientation conducive to electron tunneling from the electrode to the enzyme.

Further evidence supporting proper Laccase functionalization on the electrode comes from SEM analysis.

(a) Scale: 2 µm.   **(b)** Scale: 200 nm.
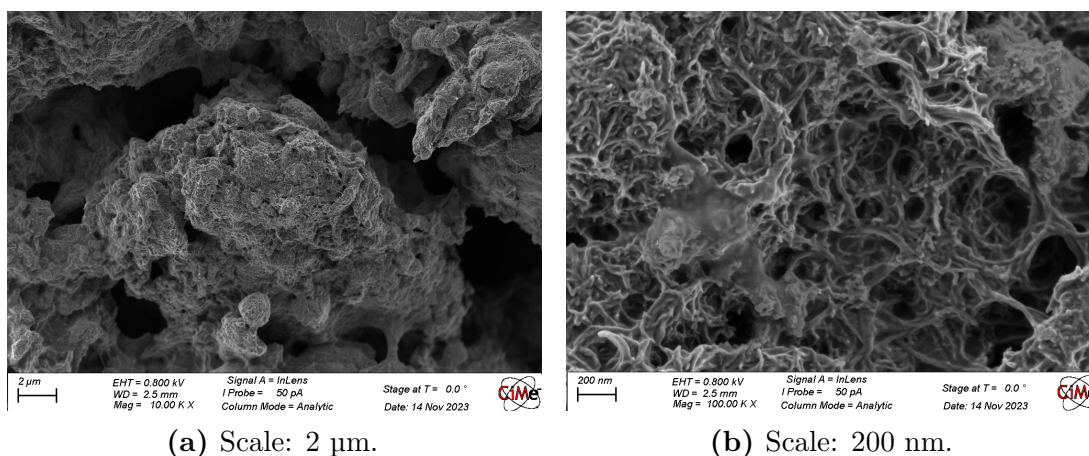
Figure 4.6: SEM pictures of Laccase deposited on MWCNTs.

When comparing the electrode with and without laccase deposited on MWCNTs at a scale of 2 micrometers (Figure 4.6a and Figure 4.3a), no apparent differences are observable. However, conducting the same comparative analysis at a scale of

Table 4.1: Mean and standard deviation of functionalized MWCNTs.

	Mean diameter (nm)	Standard deviation diameter (nm)
MWCNTs	19.57	3.02
MWCNTs and Laccase	28.18	4.23

200 nanometers (Figure 4.6b and Figure 4.3b), where MWCNTs are visible in their form, reveals an increase in the diameter of MWCNTs due to enzyme deposition. Specifically, calculating the diameter of the functionalized MWCNTs and comparing it with the diameter of naked MWCNTs shows an increase in diameter of 8.61 nm (all the results are shown in Table 4.1). Considering that the volumetric dimensions of Laccase are 6.5x5.5x4.5 nm^3 [65], it is evident that the diameter increase aligns with the protein's size when arranged on each side of the MWCNTs.

In conclusion, the analysis of cathode functionalization indicates that the enzyme seems to have been appropriately deposited on the MWCNTs, and its electrochemical activity has been detected. However, optimizing the concentration of Laccase could be a good starting point to enhance the performance observed in the differential pulse voltammetry. Additionally, analyses in oxygen-deprived or oxygen-saturated solutions may provide further insights into the study of the thus-functionalized electrode.

4.1.3 Anode: Direct electrons transfer method

As previously defined, the initial attempt to functionalize the anode was made through dropcasting Glucose Oxidase on the electrode already functionalized with MWCNTs. The objective is to analyze the possibility of achieving direct electron transfer through this mechanism. In this section, correspondent results and discussion will be shown.

The initial comparison that can be appreciated concerns the electrochemical effect of Glucose Oxidase when dropcasted on MWCNTs in PBS. In Figure 4.7b the cyclic voltammetry results at different scan rates are presented for the electrode functionalized with MWCNTs and Glucose Oxidase, while in Figure 4.7a the same analysis was performed for the electrode functionalized only with MWCNTs. Both measurements were conducted with the electrode immersed in PBS. To visualize the difference in cyclic voltammetry between the presence and absence of the enzyme Glucose Oxidase, the two respective cyclic voltammetry profiles, conducted with a scan rate of 100 mV/s, are depicted in the figure 4.8.

From the last figure mentioned, it is possible to notice a distinct peak around -500 mV when Glucose Oxidase is present. To explain what it is possible to observe here, it is necessary to take a step behind. The redox center crucial for the enzymatic
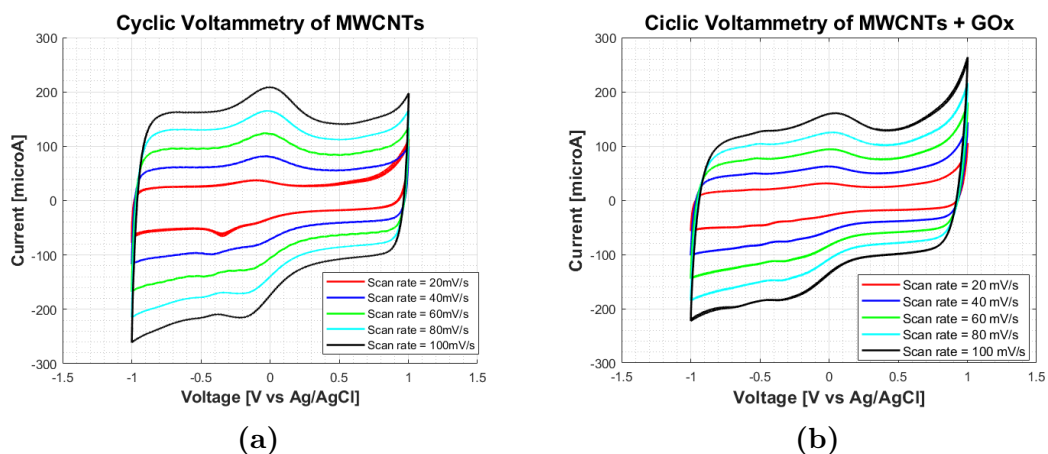
Figure 4.7: Comparison between Cyclic voltammetry in PBS on MWCNTs Electrode in **(a)** and Cyclic voltammetry in PBS on MWCNTs+GOx Electrode in **(b)**
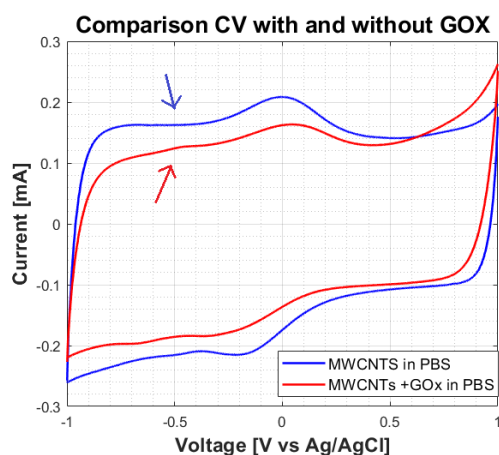
Figure 4.8: Comparison between CV with and without GOX on MWCNTs.

activity of Glucose Oxidase is the flavin adenine dinucleotide (FAD) cofactor [55]. The underlying reaction involving the FAD cofactor within the enzyme's functional mechanism is expressed as follows:

$$\text{GOX(FAD)} + 2\text{H}^+ + 2e^- \rightarrow \text{GOx(FADH}_2) \tag{4.1}$$

Considering that the standard potential of FAD at pH 7 is documented at -0.46 V [66], and considering the absence of this peak in the absence of Glucose Oxidase, it is reasonable to attribute this peak to the electrochemical activity of the FAD cofactor. It is crucial to note that this observed peak is unrelated to the oxidation of

glucose, as glucose is not present in the solution during the conducted CV analysis. Instead, it solely reflects the electrochemical activity of the GOx enzyme.

Consequently, the next step aims to analyze whether the addition of glucose in solution at different concentrations reveals the effects of a potential electron transfer. As explained in the corresponding section of the methodology, this analysis was conducted through cyclic voltammetry in PBS with varying concentrations of glucose and a scan rate of 20 mV/s. Figure 4.9 provides an example, referring to an electrode on which MWCNTs have been deposited and a GOx concentration of 5 mg/mL is drop-casted on them.
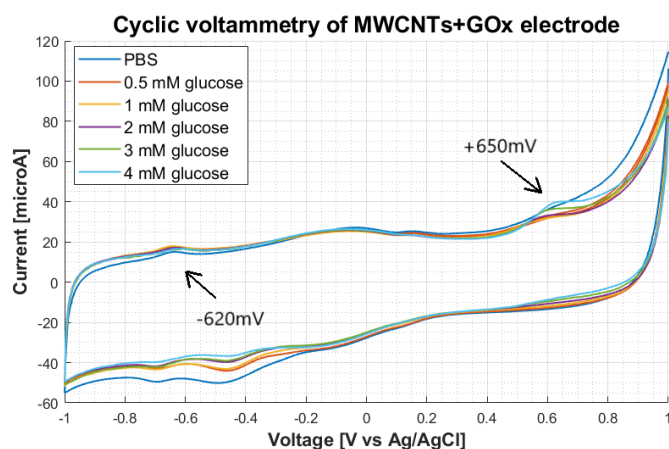
Figure 4.9: CV of MWCNTs and GOx in different glucose concentration.

In Figure 4.9, two oxidation peaks, highlighted with arrows, are evident. It is crucial to note that the corresponding reduction peaks are also present, but since the operation of interest concerns the oxidation of glucose, they are identified without detailed analysis. Since the window on which the cyclic voltammetry is performed is particularly broad, given the exploratory nature of the analysis, baseline subtraction is performed on them to verify the increase of the peak with the increment in glucose concentration.

The first oxidation peak analyzed is the same as previously discussed and related to the electrochemical activity of Glucose Oxidase, it is located around -620 mV and it is shown in Figure 4.10a. It is expected that if direct electron transfer occurs, this peak will grow with increasing glucose concentration, consistent with enzymatic detection. However, Figure 4.10a shows that when the concentration of GOx deposited on the electrode is 5 mg/mL, this expected increase in the peak does not occur.

This examination extends beyond a concentration of Glucose Oxidase equal to 5 mg/mL; it also involves concentrations of 2 mg/mL, 7 mg/mL, and 12 mg/mL.

Rather than presenting individual series of peaks for each concentration separately, they are consolidated in Figure 4.10b as calibration curves. Each concentration is related to a distinct curve which provides insight into the relationship between the observed current peak height and the concentration of glucose in the PBS solution. This organization allows for a comprehensive understanding of the electrochemical response across varying enzyme concentrations.
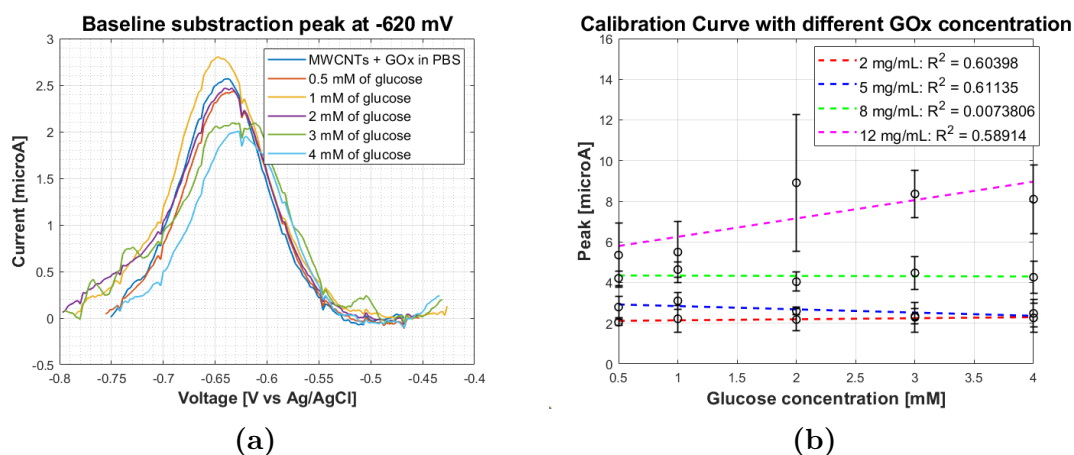
Figure 4.10: (a): oxidation peak at -620 mV after baseline subtraction in different glucose concentration. **(b)** : correspondent calibration curves for different GOx concentration.

Based on these collected data, several observations can be made. Firstly, observing the first point of each calibration curve, related to a glucose concentration of 0.5 mM, it is evident that the mean value of current increases with the increasing concentration of GOx deposited on the electrode. Since this peak is related to the activity of the FAD cofactor within the Glucose Oxidase enzyme, it confirms the increase in the number of such activities and therefore the actual increase in the quantity of Glucose Oxidase present.

However, for concentrations of GOx equal to 2 mg/mL, 5 mg/mL (as mentioned earlier), and 8 mg/mL, there is no increase in the oxidation peak with the increasing glucose concentration. Regarding a concentration of 12 mg/mL, the line interpolating the points has a positive trend, suggesting an increase in the peak. However, the solutionent of determination of the line suggests that the set of points is not well described by a linear trend, and therefore, more than representing the enzymatic kinetics, it seems to be dictated by noise.

The same analysis was conducted on the oxidation peak at +650 mV.

From Figure 4.11a, it is evident that this peak increases with the growing concentration of glucose in the solution when the concentration of GOx deposited on
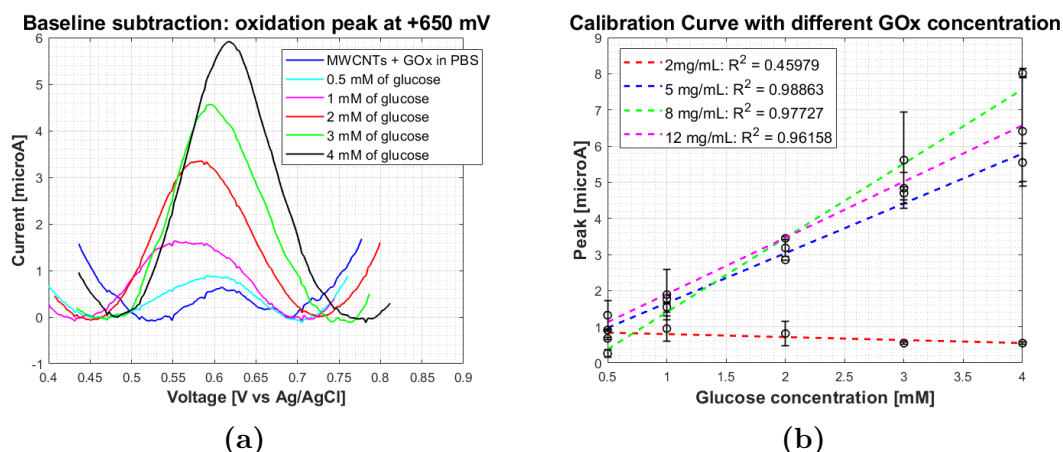
Figure 4.11: **(a)**: oxidation peak at +650 mV after baseline subtraction in different glucose concentration. **(b)** : correspondent calibration curves for different GOx concentration.

the electrode is equal to 5 mg/mL. Furthermore, the overall analysis of the generated calibration curves, as shown in Figure 4.11b, confirms this increasing linear trend, with the exception of the concentration of 2 mg/mL of GOx. Considering the very low concentration of Glucose Oxidase in this latter case, the results suggest that the amount of enzyme is so minimal that it does not allow for a noticeable manifestation of meaningful outcomes. The coefficients of determination calculated for the regression lines further support the observation that the data show a growing linear trend with the concentration of glucose.
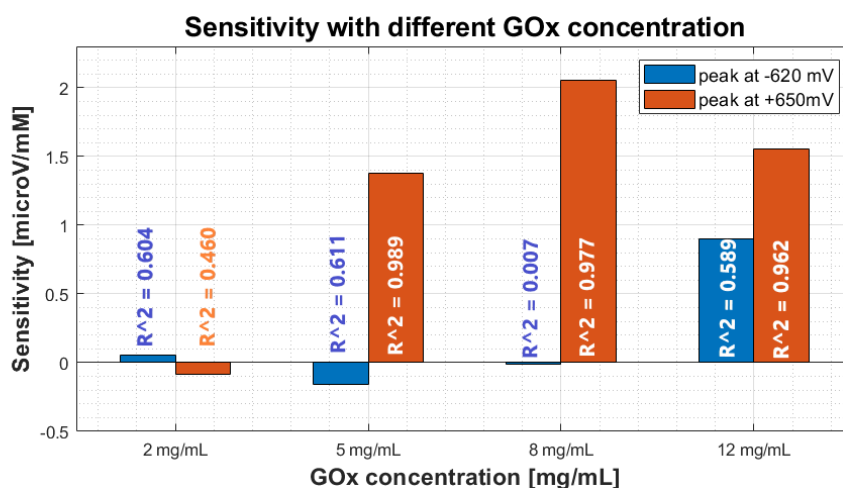
Figure 4.12: Sensitivity of the glucose detection.

To summarize the obtained results regarding the two peaks, Figure 4.12 illustrates the slope of each regression line for every Glucose Oxidase concentration and each measured peak. This slope represents the sensitivity of glucose detection. The significance of this coefficient lies in its indication that higher sensitivity results in a greater measured current for an equal variation of glucose concentration. The analysis is relevant because the goal is to achieve direct electron transfer, aiming for the highest possible current at the same concentration of glucose.

The coefficient of determination, reported in the same figure, provides insights into the appropriateness of sensitivity concerning a good linear fitting. Upon analysis, it becomes apparent that the peak at -620 mV does not seem to be representative of enzymatic kinetics because of the very low value of the coefficient of determination. In contrast, concerning the peak at +650 mV, the sensitivity increases with the concentration of GOx until reaching a peak at 8 mg/mL and then decreases.

On the other side, the results of the morphological characterization are shown in Figure 4.13a, 4.13b, 4.13c and 4.13d for the respective concentrations of 2 mg/mL, 5 mg/mL, 8 mg/mL, and 12 mg/mL of GOx.

For a more quantitative evaluation, the mean diameter and the correspondent standard deviation of MWCNTs before and after Glucose Oxidase deposition were calculated for each concentration and displayed in Table 4.2.

Table 4.2: Mean and standard deviation of functionalized MWCNTs with GOx.

	Mean diameter [nm]	Standard deviation diameter [nm]
MWCNTs	19.57	3.02
MWCNTs + 2 mg/mL GOx	22.58	5.39
MWCNTs + 5 mg/mL GOx	26.01	3.22
MWCNTs + 8 mg/mL GOx	27.90	5.13

The SEM images and the corresponding quantitative evaluation of the diameter seem to support the considerations drawn earlier. Specifically, for a GOx concentration of 2 mg/mL, the calculated average diameter of MWCNTs does not undergo a significant increase compared to bare MWCNTs, with a difference of approximately 3 nm. Given that the enzyme Glucose Oxidase measures 6.0 x 5.2 x 3.7 nm^3 [55], the observed increase in diameter on MWCNTs at 2 mg/mL suggests insufficient coverage, as it should ideally double the enzyme's dimensions for complete coverage. In light of these data, the notion of a "poor" deposition in terms of concentration from the GOx perspective makes sense, providing context for the corresponding calibration curve shown in Figure 4.11b in red in which any outcomes was visible.

However, at concentrations of 5 and 8 mg/mL of GOx, the diameter experiences

(a) 2mg/mL of GOx.

(b) 5 mg/mL GOx.

(c) 8 mg/mL GOx.

(d) 12 mg/mL of GOx.
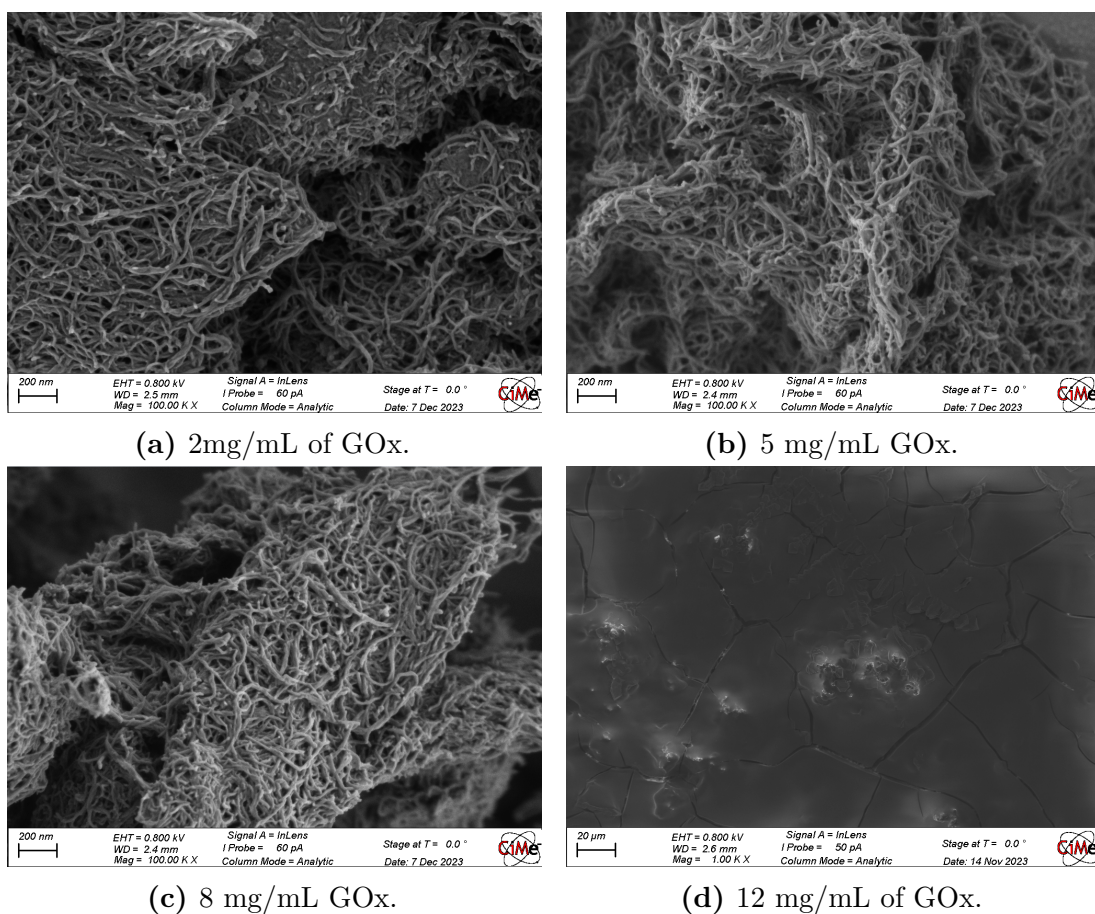
Figure 4.13: SEM pictures of GOx deposited on MWCNTs in different concentration.

a more substantial increase, around 7 nm. This indicates a more robust and measurable coating of the carbon nanotube with the enzyme. In the corresponding calibration curves (Figure 4.11b in blue and green, respectively), the sensitivity is higher, revealing increasing enzymatic activity.

Finally, in the case of a concentration of 12 mg/mL, as depicted in Figure 4.13d, the electrode appears to be entirely covered by a membrane, potentially reducing the efficiency of GOx activity. This is confirmed by the fact that the sensitivity of the corresponding calibration curve, in magenta in Figure 4.11b, is lower than the previous ones despite the higher concentration of GOx. This reveals that an excessive enzyme concentration can be detrimental to the final performance, emphasizing the importance of carefully tuning this parameter.

From the joint analysis of these oxidation peaks, it is possible to draw significant conclusions about what is happening in the proposed system. As mentioned in

the chapter 2 concerning direct electron transfer, the process of electron transfer from glucose to the electrode through oxidation is competitive with oxygen, which represents the natural substrate of GOx. Specifically, as shown in the relation 4.1, the FAD cofactor present in Glucose Oxidase acts as the first electron acceptor, becoming $FADH_2$. To return to its initial form, the cofactor can react by releasing the mentioned electrons to the electrode, determining the so-called DET, or it can react with molecular oxygen according to reaction 4.2, giving rise to hydrogen peroxide that accumulates in solution.

$$GOX(FADH_2) + O_2 \rightarrow GOx(FAD) + H_2O_2 \tag{4.2}$$
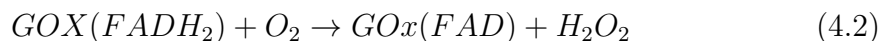
Compared to an Ag/AgCl electrode, hydrogen peroxide is oxidized at a potential of about 650 mV [67].

$$H_2O_2 \rightarrow O_2 + 2H_2O + 4e^- \tag{4.3}$$

Consequently, the peak identified in the cyclic voltammetry depicted in Figure 4.9 around this value and then further analyzed in Figures 4.11a and 4.11b proves to be related to this oxidation mechanism. This peak increases with increasing glucose concentration as the corresponding activity of Glucose Oxidase increases, producing greater amounts of hydrogen peroxide that can subsequently be oxidized. This behavior is typical of so-called first-order glucose sensors [67].

The identification of this peak confirms that Glucose Oxidase is active and effective in its action of oxidizing glucose. However, it also indicates that MWCNTs are not sufficiently bound to the redox center of GOx to allow such efficient electron transfer to the electrode. This is highlighted by the fact that, despite the peak related to hydrogen peroxide increasing with glucose concentration, the same does not occur for the peak related to the FAD cofactor.

This observed behavior may not be advantageous for the operation of the biofuel cell. Indeed, moving from cyclic voltammetry (CV) to the context of galvanic cells, the potential that drives oxidation and reduction is no longer externally generated but must be spontaneously generated by the system. However, since it is the oxidation of hydrogen peroxide determines the transfer of electrons to the electrode, and no longer the oxidation of glucose, the value of the Gibbs free energy difference underlying the spontaneity of the reaction is different from the one intended to obtain, as is the physical principle involved.

Furthermore, it is important to remember that to enable efficient electron transfer from the anode to the cathode, the potential at which oxidation occurs (anode) must be lower than the potential at which reduction occurs (cathode). In this case, this limit is not respected, as the oxidation of hydrogen peroxide occurs around 650 mV, while the reduction of Laccase occurs around 600 mV with respect Ag/AgCl.

To conclude, I would like to focus on the hydrogen peroxide generation at the anode in the context of biofuel cells. Being a competitive process with oxygen, hydrogen peroxide is always produced in the presence of oxygen, limiting the electron transfer process compared to when oxygen is absent. The role of oxygen in solution is critical for the biofuel cell: on one hand, it is essential for the proper functioning of the cathode, on the other hand, it is detrimental to the anode's performance as it engages in a competitive process with electron transfer to the electrode [36]. This could be one of the reasons why microfluidic-based biofuel cells, which keep glucose and oxygen separated and can accurately regulate these quantities in the two anodic and cathodic compartments, represent a winning solution capable of significantly increasing the amount of power produced. It is also relevant to mention that there are enzymes that, unlike Glucose Oxidase, do not involve the use of oxygen as a natural substrate, such as Glucose Dehydrogenase [36, 53]. However, Glucose Dehydrogenase is accompanied by certain drawbacks, including reduced long-term stability compared to GOx. Additionally, it has undergone less extensive research and application [53]. Consequently, it has not been considered as the primary choice for enzyme selection in the context of implantable devices.

Going back to the issue of hydrogen peroxide, it is crucial to mention that when generated by the process mentioned above, it tends to accumulate near the anode, hindering the access of glucose and ions to the electrode interface. This unintentional membrane-like formation imposes limitations on the performance of the biofuel cell at the anode. Notably, in the study by A. Zebda et al. [40], this issue is addressed by introducing another enzyme, catalase, alongside Glucose Oxidase at the anode. Catalase plays a role in decomposing hydrogen peroxide to generate molecular oxygen and water. This strategic inclusion aims to enhance the availability of oxygen at the cathode for the reduction process.

4.1.4   Anode: mediated electrons transfer method

As the attempt to achieve direct electron transfer seems to be inefficient or not occurring, the insertion of a mediator into the system has been tried, namely ferrocenemethanol, with the role of facilitating electron transfer. This option was not considered as the first choice because the introduction of an additional element into the system increases the complexity of the process that must occur at the electrode and influences its stability. Additionally, it reduces the theoretical open circuit potential in the biofuel cell. In this section outcomes achieved through the utilization of ferrocenemecethanol as a mediator are shown and the correspondent discussion is carried out.

The easiest way to perform an initial check on the functioning of the system using the mediator is to introduce the freely moving mediator into the solution and perform electrochemical analysis through cyclic voltammetry in the presence of

different concentrations of glucose. The result of this analysis, shown in Figure 4.14,
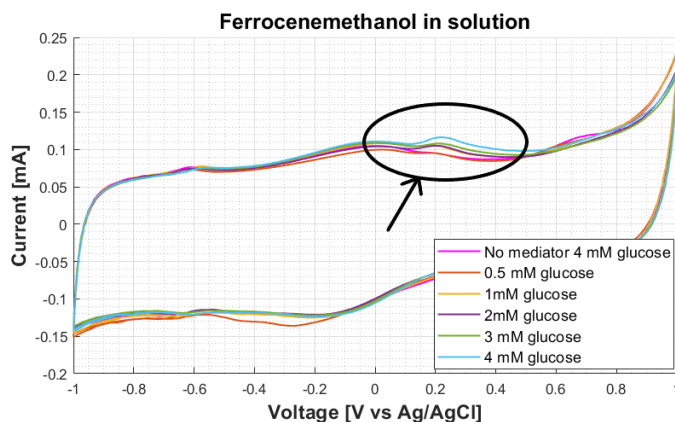
Figure 4.14: CVs with ferrocenemethanol in solution.

reveals the presence of an oxidation peak around 200 mV, while the reduction peak is not visible. From the peak analysis performed through baseline subtraction and shown in Figure 4.15a, it is evident that with an increase in glucose concentration, the observed peak also increases. In this case, the calibration curve is calculated as shown in Figure 4.15b From the calculation of the corresponding sensitivity, it is noteworthy that it is equal to 3.5 µV/mM: to make a comparison, higher than what was obtained previously through the oxidation of H_2O_2.
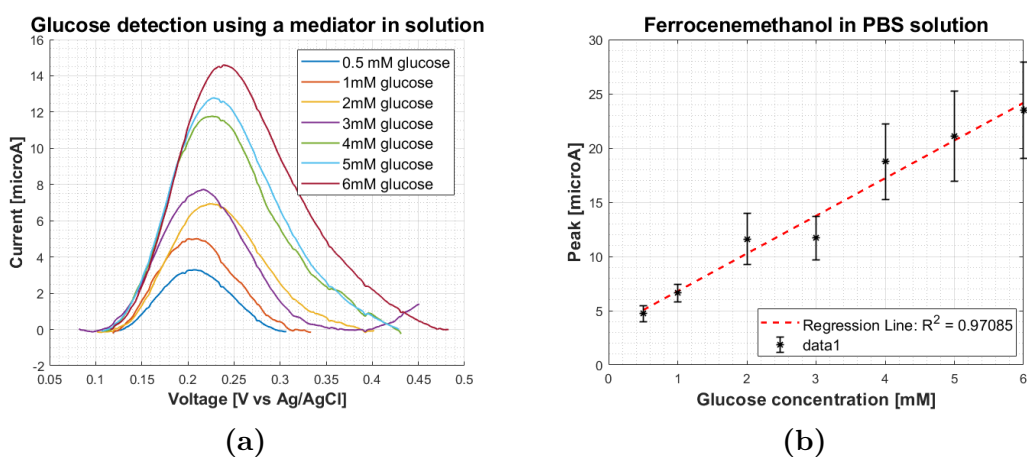
Figure 4.15: **(a)**: baseline subtraction of ferrocene-methanol oxidation peak. **(b)** : correspondent calibration curves to analyse glucose sensitivity.

The observed increase in sensitivity aligns with expectations when introducing a mediator into the solution. Mediators, originally employed in glucose sensing, are

designed to enhance sensitivity, providing a more precise measurement of glucose concentration [36]. This anticipated behavior arises from overcoming the limitations associated with direct electron transfer, where the enzyme's redox center needs to be near the conductive electrode (within 2 nm), posing challenges in stabilizing the enzyme in the correct orientation. While introducing mediators adds complexity to the system, it proves effective in improving sensitivity.

Despite the efficient mediated electron transfer achieved through this strategy, it is important to emphasize that leaving the mediator free in solution is complex in terms of implantable devices application. Indeed, since oxygen and glucose are in the same chamber, the mediator would cause a kind of short circuit in the biofuel cell, preventing power generation.

In this case, the strategy to be employed is to secure the mediator to the electrode. In this scenario, a dropcasting strategy of ferrocenemethanol between Glucose Oxidase enzyme and MWCNTs has been adopted for simplicity. The results, depicted in Figure 4.16, are based on four successive CV scans (with the first scan discarded) conducted in the same PBS solution.
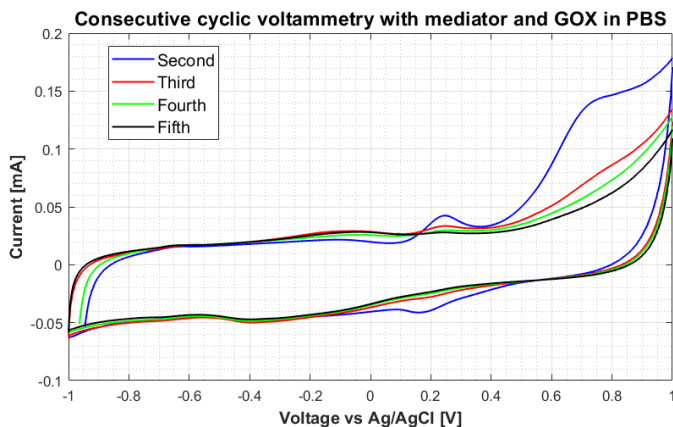
Figure 4.16: CVs of dropcasting of mediator on electrode.

The identified peaks are analyzed using baseline subtraction to highlight the trends of successive CV peaks in the same solution (Figure 4.17a and 4.17b).

The analysis of these subsequential CV immediately highlights a significant issue. Indeed, without changing the setup, performing successive cyclic voltammetry in PBS shows a decrease in the observed oxidation and reduction peaks. If this observation is combined with the fact that during the experiment, the mediator is observed detaching from the electrode surface and entering the solution (indicated by a yellowish color change in the solution), it is evident that the reduction in peak intensity is due to the mediator detaching from the electrode. This experiment,

51

(a)   **(b)**
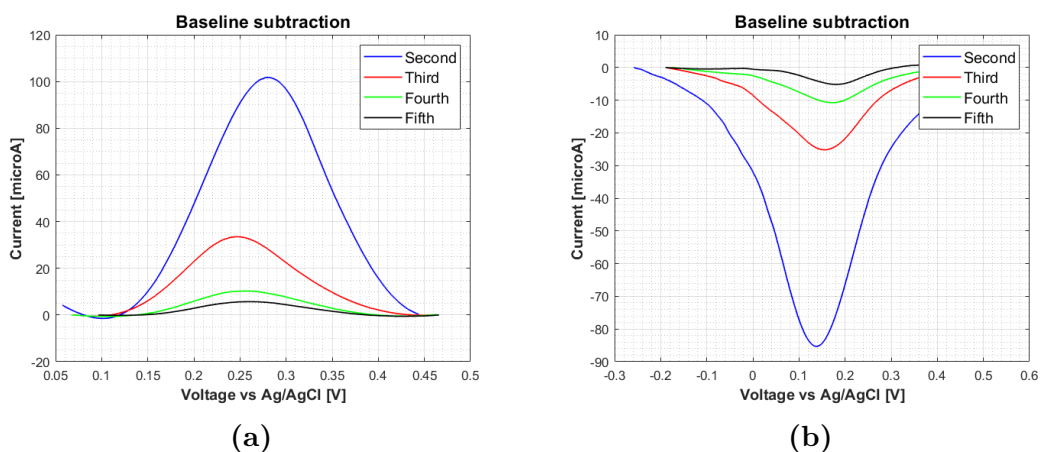
Figure 4.17: Oxidation peak **(a)** and reduction peak **(b)** after baseline subtraction when ferrocenemethanol is on the electrode during consecutive cyclic voltammetry

conducted for various concentrations of ferrocenemethanol, is summarized in Figure 4.18, where the decrease in oxidation and reduction peaks in successive cyclic voltammetry is evident. This highlights the need, as expected, for the use of a more effective stabilization technique.
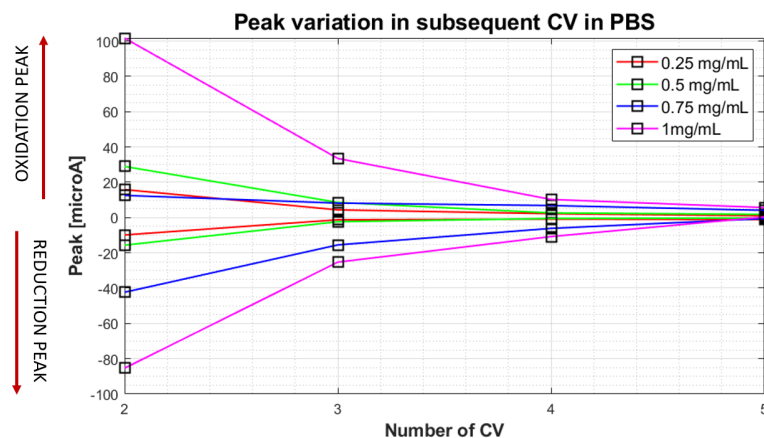
Figure 4.18: Trend of oxidation and reduction peaks.

The results obtained by adding different concentrations of glucose to the solution are not reported here, as distinguishing the potential increasing trend in peak intensity due to sensing increasing concentrations of glucose from the decreasing trend caused by mediator loss proves to be complex.

Despite the instability of the mediator encountered, it was still decided to test this electrode as part of the biofuel cell later on. CV is useful to verify whether

electron transfer occurs towards the electrode, but it is a different process than in the biofuel cell. It is reasonable to assume that applying an external potential to the electrode increases the instability of the material deposited on it. However, this does not negate the earlier considerations regarding the need for a more robust stabilization methodology for the mediator.

4.2 Integration to a Biofuel cell

In this section, results about the construction of the biofuel cell by coupling the cathode and the anode will be shown and the correspondent discussion will be carried out.

Regarding the biofuel cell built with a mediator-free anode (i.e., absence of the ferrocenemethanol mediator), the results presented in Figure 4.19 reveal that OCP recorded when immersed in 500 mM of glucose is -90 mV. The negative sign indicates an inverted polarity, implying that, instead of the cathode being more positive than the anode, the situation is reversed. This outcome indicates that the biofuel cell constructed in this manner does not operate as expected.
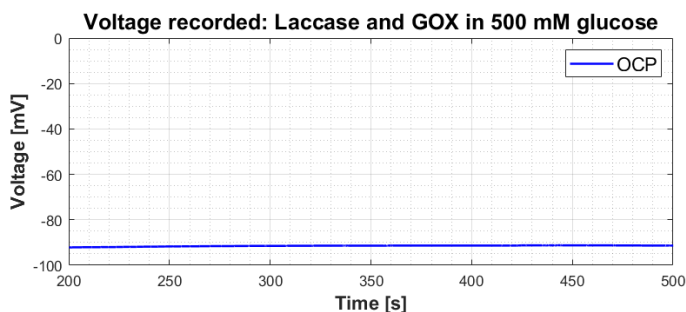
Figure 4.19: Voltage recorded of a biofuel cell composed by anode with MWCNTs and GOx and cathode with MWCNTs and laccase.

By connecting the anode made of MWCNTs, GOx and ferrocemethanol and the cathode made of MWCNTs and Laccase, the voltage recorded with different resistances applied when the biofuel cell is working in PBS and in 500mM glucose is shown respectively in Figures 4.20a and 4.20b. This results are notably more promising. As shown in Figure 4.20a, immersing the biofuel cell in a PBS-only solution generates a positive potential, around 100 mV, in the absence of glucose. This effect is attributed to the electrochemical activity of the mediator, glucose oxidase, and Laccase enzymes, along with the reaction of PBS with MWCNTs. This potential promptly drops to 40 mV when a resistance is inserted in parallel with the system.

When immersed in 500 mM of glucose, the recorded open-circuit potential

53

stabilizes at approximately 300 mV (Figure 4.20b). The significant difference in measured potential between the biofuel cell in PBS and 500 mM glucose suggests that glucose is indeed contributing to the potential, and it's not solely the exclusive activity of the mediator. Furthermore, by inserting a series of resistances in parallel, the potential when a load is connected to the system can be recorded. Since this value does not rapidly decrease to zero, it is now feasible to proceed to the subsequent steps of biofuel cell characterization.
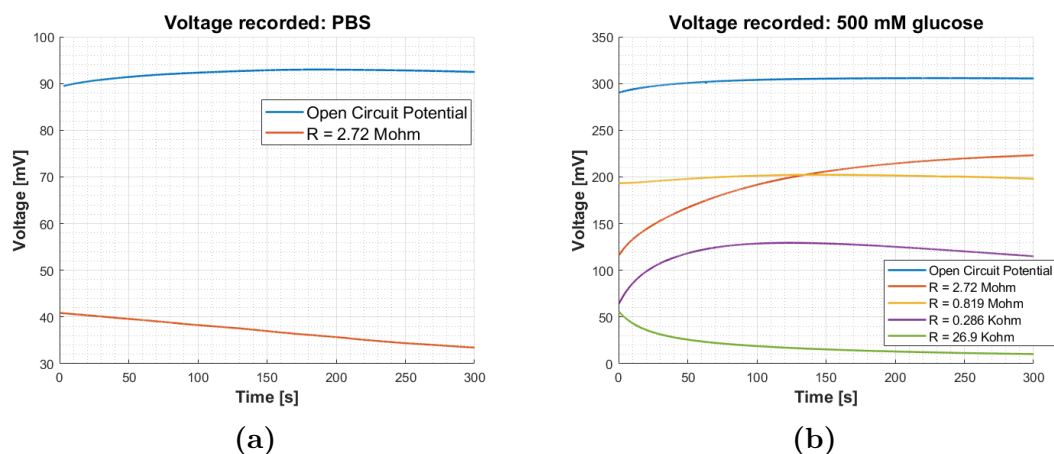
Figure 4.20: Voltage recorded during the test of the biofuel cell when ferrocenemethanol is employed. In **(a)** the test is conducted in PBS while in **(b)** in 500mM of glucose

Figure 4.21 illustrates the relationship between the measured voltage between cathode and anode in the presence of a certain value of resistance in parallel. The recorded voltage after 5 minutes of measurement is used to ensure comparability between measurements.

In Figure 4.22, the power density curve is presented on the left, and the polarization curve is on the right. Initial observations indicate that the results align with the expected behavior in biofuel cell characterization. Particularly, the power density curve exhibits a parabolic trend, while the calibration curve highlights that the current flowing between the two electrodes decreases as the voltage across the resistance increases. For a more precise definition of the curves and improved characterization of the biofuel cell, using a broader range of resistance values in future works is recommended. The analysis reveals that the maximum power density reached is 0.38 $\mu W/cm^2$, achieved at a voltage of approximately 200 mV. The power density value shows that these preliminary results are far away from the current state-of-the-art in biofuel cells. This becomes even clearer when considering that the measurements were taken at glucose concentrations much higher than physiological levels. However, they confirm the functionality of the system with the
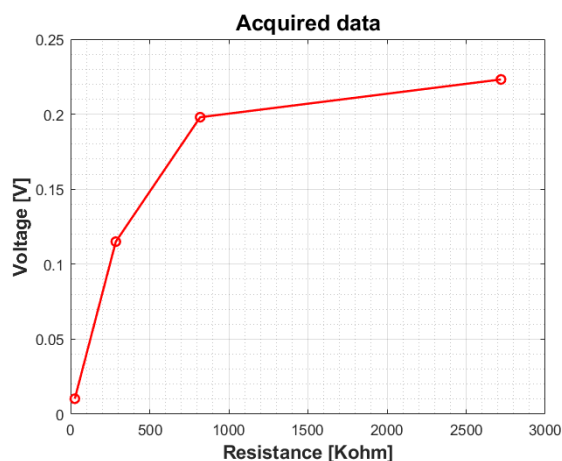
Figure 4.21: Voltage measured with respect to resistance applied.
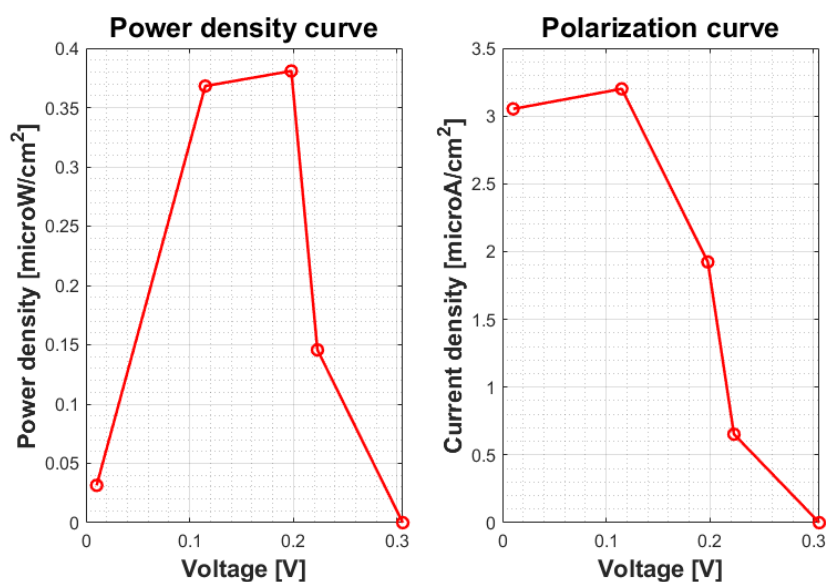
Figure 4.22: Power density and polarization curve.

materials used and establish a foundation for its enhancement and optimization.

Another crucial consideration is that the recorded open-circuit potential is low relative to the state of the art, leading to a low operative voltage as well. This outcome was somewhat expected, as transitioning from implementing a biofuel cell based on direct electron transfer to mediated electron transfer results in a decrease in the open-circuit potential. The cause of this phenomenon can be attributed to the mediator facilitating the electron transfer from Glucose Oxidase to the electrode. The mediator must have a more positive redox potential than that of the consumed

glucose to act as the driving force for electron transfer. However, the discrepancy between these redox potentials introduces an activation overpotential, reducing the observed open-circuit potential below the theoretical maximum determined by the formal potential difference between the fuel and oxidant [68]. Since literature includes biofuel cells based on mediated electron transfer with an open-circuit potential exceeding 500 mV, it is advisable to align the choice of mediator in this direction to enhance the system in terms of the produced voltage [36]. Indeed, the choice and stabilization of the mediator play a key role in this context. As this is a preliminary study, this aspect was not considered in the initial selection but represents an excellent starting point for system optimization.

Another alternative, following optimization, is to explore the option of connecting two biofuel cells in series to increase the generated potential. This approach is relevant in the field of active implantable devices where the required voltage typically exceeds 1 V, addressing challenges encountered even by state-of-the-art biofuel cells [69].

Furthermore, it is essential to note that, even in this case, the constructed biofuel cell exhibits considerable instability over time. After completing an entire set of measurements, the loss of pieces from the layer consisting of ferrocenemethanol and MWCNTs was observed in the solution. This rendered the biofuel cell non-functional and once again highlighted the challenges related to electrode stabilization.

Chapter 5

Future work

While the current research has provided valuable insights, there are several avenues for future exploration and enhancement in the field of biofuel cells for implantable sensors.

Firstly, I believe it is necessary to conduct additional measurements related to the stability of the developed biofuel cell. It would be interesting, in particular, to investigate the trend of the open circuit potential to assess the long-term performance of the biofuel cell. This could be achieved using the same setup mentioned for the biofuel cell testing, keeping the cathode and anode connected and continuously recording the detected potential until it stabilizes near zero. In this context, it is crucial to continuously provide glucose to ensure that the decrease in open circuit potential is attributed to a decline in performance rather than the absence of glucose.

Furthermore, it is important to note that these are preliminary results, stemming from the realization of an initial prototype of the biofuel cell. Therefore, it is advisable to engage in an optimization process aimed at improving electron transfer and stability, both from the perspective of the anode, where the use of Glucose Oxidase without a mediator presents complications, and the cathode, where the main challenge arises from the limited solubility of oxygen in the plasma, and more generally in PBS. From the obtained results, the electrode designated as the anode has proven to be the most intricate concerning its role in electron transfer. Since the results indicate that direct electron transfer is inefficient with the employed methodology, future project developments will primarily focus on optimizing mediated electron transfer, which has shown more promising preliminary results. However, the instability of the mediator on the electrode emphasizes the need for a more thorough investigation into stabilization technologies. In this regard, an effective approach may involve utilizing redox polymer complexes to construct a three-dimensional matrix capable of enclosing or binding electroactive biomaterials, thereby confining them on the electrode surface [36]. Redox polymers, capable of

undergoing reversible oxidation and reduction processes, act as mediators, with the redox center localized in the polymer's side chain or main backbone. At the same time, due to their polymer nature, they can be employed to entrap other materials, such as enzymes or nanomaterials in the case of biofuel cells. Thanks to these features, films composed of these redox polymers have demonstrated high mechanical and redox stability, along with rapid electron transfer [70]. Furthermore, if this technique proves successful, it would be interesting to analyze the performances in the case where a mediator is also added at the cathode level, considering the low concentrations of oxygen in solution and the consequent need to make the most of the available oxygen.

Then, the biofuel cell developed in this thesis utilized a commercial screen-printed electrode as electrode support. This choice was made for simplicity and to focus on the most critical steps of constructing a biofuel cell, such as electron transfer. However, the commercial screen-printed electrode has its limitations. As it is a commercially available product, the shape and dimensions of the electrode cannot be predefined. This is certainly a limitation, especially when considering the scalability of the biofuel cell, which is crucial for miniaturized implantable sensors. In other words, in biofuel cell applications reported in the literature, power is often expressed as power density over area. However, electrode dimensions are frequently undefined, or there is confusion in reporting geometric or three-dimensional areas obtained from electrode functionalization. Additionally, no studies have been found to demonstrate that the value obtained is effectively scalable with electrode dimensions, and an investigation in this regard would be relevant for miniaturized implantable devices.

Without deviating from the methodology chosen in this thesis, the screen printing technique is suitable for the fabrication of customized electrodes. It is a low-cost fabrication technique where conductive ink is deposited layer by layer over a substrate using screen frames. This provides more freedom and flexibility regarding substrate material, inks, sizes, and design, making it suitable for large-scale manufacturing and experimentation purposes[71].

Chapter 6

Conclusion

In conclusion, this preliminary investigation in the field of biofuel cells within the context of implantable sensors has provided some insights into the feasibility and challenges that a biofuel cell must overcome to serve as the power source for miniaturized implantable sensors. Firstly, it has highlighted that it is theoretically possible to derive energy from the blood, even if generating limited power under physiological conditions (1 µW/cm^2). This power value increases when considering biofuel cells operating at higher glucose concentrations or when employing microfluidic techniques to separate oxygen from glucose, a challenging strategy in the context of implantable devices. From this investigation, it has also emerged that enzymatic biofuel cells are the most suitable for implantable devices, and that nanomaterials such as carbon nanotubes are useful for increasing the produced power and electron transfer efficiency.

The implementation of the biofuel cell prototype has demonstrated the ability to generate a power density of 0.38 µW/cm^2 at 200 mV using selected materials such as carbon nanotubes, Glucose Oxidase, and ferrocene-methanol at the anode, and carbon nanotubes and Laccase at the cathode. Glucose has proven to be the determining factor for energy harvesting, as without it, the recorded potential value is significantly lower, confirming that the biofuel cell behaves as expected. Despite these results falling short of cutting-edge technologies and the physiological concentration of glucose for which the device was designed, they pave the way for a subsequent optimization process.

References

[1] Sandro Carrara. «Body dust: Well beyond wearable and implantable sensors». In: *IEEE Sensors Journal* 21.11 (2020), pp. 12398–12406 (cit. on pp. 1, 2).

[2] Gian Luca Barbruni, Paolo Motto Ros, Danilo Demarchi, Sandro Carrara, and Diego Ghezzi. «Miniaturised wireless power transfer systems for neurostimulation: A review». In: *IEEE Transactions on Biomedical Circuits and Systems* 14.6 (2020), pp. 1160–1178 (cit. on p. 1).

[3] Arushi Chauhan and Pramod Avti. «Implantable Biofuel Cells for Biomedical Applications». In: *Biofuel Cells: Materials and Challenges* (2021), pp. 69–95 (cit. on pp. 2, 13, 16).

[4] Abdelkader Zebda et al. «Single glucose biofuel cells implanted in rats power electronic devices». In: *Scientific reports* 3.1 (2013), p. 1516 (cit. on pp. 2, 16, 70).

[5] Benjamin I Rapoport, Jakub T Kedzierski, and Rahul Sarpeshkar. «A glucose fuel cell for implantable brain–machine interfaces». In: *PloS one* 7.6 (2012), e38436 (cit. on pp. 2, 15, 18, 19, 71).

[6] Amay J Bandodkar et al. «Soft, stretchable, high power density electronic skin-based biofuel cells for scavenging energy from human sweat». In: *Energy & Environmental Science* 10.7 (2017), pp. 1581–1589 (cit. on pp. 2, 72).

[7] Evgeny Katz and Paolo Bollella. «Fuel cells and biofuel cells: From past to perspectives». In: *Israel Journal of Chemistry* 61.1-2 (2021), pp. 68–84 (cit. on p. 4).

[8] Yulia Mariana Tesa Ayudia Putri, Jarnuzi Gunlazuardi, Yoki Yulizar, Rahmat Wibowo, Yasuaki Einaga, and Tribidasari A Ivandini. «Recent progress in direct urea fuel cell». In: *Open Chemistry* 19.1 (2021), pp. 1116–1133 (cit. on pp. 4, 9).

[9]   *Chem.Libretext: Gibbs (free) energy.* URL: https://chem.libretexts.org/
      Bookshelves/Physical_and_Theoretical_Chemistry_Textbook_Maps/
      Supplemental_Modules_(Physical_and_Theoretical_Chemistry)/The
      rmodynamics/Energies_and_Potentials/Free_Energy/Gibbs_(Free)
      _Energy (cit. on p. 5).

[10] A-S Feiner and AJ McEvoy. «The nernst equation». In: *Journal of chemical
      education* 71.6 (1994), p. 493 (cit. on p. 5).

[11] *Chem.Libretext: Nernst Equation.* URL: https://chem.libretexts.org/
      Bookshelves/Analytical_Chemistry/Supplemental_Modules_(Analytic
      al_Chemistry)/Electrochemistry/Nernst_Equation (cit. on p. 5).

[12] *Chem.Libretext:Standard Electrode Potentials.* Chemistry, Mount Royal Uni-
      versity, Chem 1202, Unit 6: Electrochemistry, 6.2. URL: https://chem.
      libretexts.org/Courses/Mount_Royal_University/Chem_1202/Unit_6%
      3A_Electrochemistry/6.2%3A_Standard_Electrode_Potentials (cit. on
      p. 6).

[13] Jinzhe Lyu, Viktor Kudiiarov, and Andrey Lider. «Corrections of voltage loss
      in hydrogen-oxygen fuel cells». In: *Batteries* 6.1 (2020), p. 9 (cit. on p. 6).

[14] Adam Z Weber et al. «A critical review of modeling transport phenomena
      in polymer-electrolyte fuel cells». In: *Journal of The Electrochemical Society*
      161.12 (2014), F1254 (cit. on p. 6).

[15] Maarten Biesheuvel and Jouke Dykstra. *Physics of Electrochemical Processes.*
      Dec. 2020. ISBN: 978-90-9033258-1 (cit. on pp. 6, 7).

[16] Soumya Pandit and Debabrata Das. «Principles of microbial fuel cell for the
      power generation». In: *Microbial fuel cell: A bioelectrochemical system that
      converts waste to watts* (2018), pp. 21–41 (cit. on pp. 7, 11).

[17] Melissa Conrad Stöppler. *RxList, Definition of Biofluid.* 6.11.2023. URL:
      https://www.rxlist.com/biofluid/definition.htm (cit. on p. 7).

[18] *American society of hematology: Blood Basics.* Access: 12.11.2023. URL: h
      ttps://www.hematology.org/education/patients/blood-basics#:~:
      text=transporting%20oxygen%20and%20nutrients%20to,filter%20and%
      20clean%20the%20blood (cit. on p. 8).

[19] *SEER Training Modules, Composition of the Blood.* National Institutes of
      Health, National Cancer Institute. URL: https://training.seer.cancer.
      gov/leukemia/anatomy/composition.html (cit. on p. 8).

[20] L. Riley. *Mean fasting blood glucose, World Health Organization.* 2023. URL:
      https://www.who.int/data/gho/indicator-metadata-registry/imr-
      details/2380#:~:text=The%20expected%20values%20for%20normal (cit.
      on p. 8).

[21] Barrie Phypers and JM Tom Pierce. «Lactate physiology in health and disease». In: *Continuing education in Anaesthesia, critical care & pain* 6.3 (2006), pp. 128–132 (cit. on pp. 8, 9).

[22] Adrian O Hosten. «BUN and Creatinine». In: *Clinical Methods: The History, Physical, and Laboratory Examinations. 3rd edition* (1990) (cit. on p. 8).

[23] Takahiro Kawasaki, Hiroshi Akanuma, and Toshikazu Yamanouchi. «Increased fructose concentrations in blood and urine in patients with diabetes». In: *Diabetes care* 25.2 (2002), pp. 353–357 (cit. on p. 8).

[24] David G Cotter, Rebecca C Schugar, and Peter A Crawford. «Ketone body metabolism and cardiovascular disease». In: *American Journal of Physiology-Heart and Circulatory Physiology* (2013) (cit. on pp. 8, 9).

[25] Philipp Simons, Steven A Schenk, Marco A Gysel, Lorenz F Olbrich, and Jennifer LM Rupp. «A Ceramic-Electrolyte Glucose Fuel Cell for Implantable Electronics». In: *Advanced Materials* 34.24 (2022), p. 2109075 (cit. on pp. 8, 15, 72).

[26] Lori Laffel. «Ketone bodies: a review of physiology, pathophysiology and application of monitoring to diabetes». In: *Diabetes/metabolism research and reviews* 15.6 (1999), pp. 412–426 (cit. on p. 9).

[27] Md Estak Ahmed, Samir Chattopadhyay, Sudipta Chatterjee, and Kushal Sengupta. «Oxygen reduction reaction in enzymatic biofuel cells». In: *Oxygen Reduction Reaction.* Elsevier, 2022, pp. 427–466 (cit. on p. 10).

[28] Marine Cadet, Sébastien Gounel, Claire Stines-Chaumeil, Xavier Brilland, Jad Rouhana, Frédéric Louerat, and Nicolas Mano. «An enzymatic glucose/O2 biofuel cell operating in human blood». In: *Biosensors and Bioelectronics* 83 (2016), pp. 60–67 (cit. on pp. 10, 72).

[29] Emmanuel M Papamichael, Haralambos Stamatis, Panagiota-Yiolanda Stergiou, Athanasios Foukis, and Olga A Gkini. «Enzyme kinetics and modeling of enzymatic systems». In: *Advances in enzyme technology.* Elsevier, 2019, pp. 71–104 (cit. on pp. 10, 11).

[30] Emil Roduner. «Understanding catalysis». In: *Chemical Society Reviews* 43.24 (2014), pp. 8226–8239 (cit. on p. 10).

[31] Casanova-Moreno Jannu, Arjona Noé, and Cercado Bibiana. «Bioelectrocatalysis for biofuel cells». In: *Biofuel Cells: Materials and Challenges* (2021), pp. 1–52 (cit. on pp. 10, 13).

[32] Rustiana Yuliasni, Abudukeremu Kadier, Nanik Indah Setianingsih, Junying Wang, Nani Harihastuti, and Peng-Cheng Ma. «Introduction to Microbial Fuel Cell (MFC): Waste Matter to Electricity». In: *Biofuel Cells: Materials and Challenges* (2021), pp. 123–144 (cit. on p. 11).

[33] Let's Talk Science. *Microbial Fuel Cells*. URL: https://letstalkscience.ca/educational-resources/stem-explained/microbial-fuel-cells (cit. on p. 12).

[34] Evgeny Katz and Paolo Bollella. «Fuel cells and biofuel cells: From past to perspectives». In: *Israel Journal of Chemistry* 61.1-2 (2021), pp. 68–84 (cit. on pp. 11, 12, 15).

[35] Linlin Wang, Xiaoge Wu, BS Qi-wen Su, Rongbin Song, Jian-Rong Zhang, and Jun-Jie Zhu. «Enzymatic biofuel cell: Opportunities and intrinsic challenges in futuristic applications». In: *Advanced Energy and Sustainability Research* 2.8 (2021), p. 2100031 (cit. on p. 12).

[36] Paul Kavanagh and Dónal Leech. «Mediated electron transfer in glucose oxidising enzyme electrodes for application to biofuel cells: recent progress and perspectives». In: *Physical Chemistry Chemical Physics* 15.14 (2013), pp. 4859–4869 (cit. on pp. 13, 49, 51, 56, 57).

[37] Mireia Buaki-Sogó, Laura García-Carmona, Mayte Gil-Agustí, Leire Zubizarreta, Marta García-Pellicer, and Alfredo Quijano-López. «Enzymatic glucose-based bio-batteries: bioenergy to fuel next-generation devices». In: *Topics in Current Chemistry* 378 (2020), pp. 1–28 (cit. on p. 13).

[38] X Dominguez-Benetton, S Srikanth, Y Satyawali, K Vanbroekhoven, and D Pant. «Enzymatic electrosynthesis: an overview on the progress in enzyme-electrodes for the production of electricity, fuels and chemicals». In: *J. Microb. Biochem. Technol. S* 6 (2013), p. 007 (cit. on p. 13).

[39] Ivan Ivanov, Tanja Vidaković-Koch, and Kai Sundmacher. «Recent advances in enzymatic fuel cells: experiments and modeling». In: *Energies* 3.4 (2010), pp. 803–846 (cit. on p. 13).

[40] Abdelkader Zebda, Chantal Gondran, Alan Le Goff, Michael Holzinger, Philippe Cinquin, and Serge Cosnier. «Mediatorless high-power glucose biofuel cells based on compressed carbon nanotube-enzyme electrodes». In: *Nature communications* 2.1 (2011), p. 370 (cit. on pp. 13, 17–19, 24, 29, 49, 70).

[41] *ChemLibreTexts:Michaelis-Menten Kinetics*. 2023. URL: https://chem.libretexts.org/Bookshelves/Biological_Chemistry/Supplemental_Modules_(Biological_Chemistry)/Enzymes/Enzymatic_Kinetics/Michaelis-Menten_Kinetics (cit. on p. 14).

[42] Labster. *Michaelis-Menten Kinetics*. [Online; accessed 3-January-2024]. URL: https://theory.labster.com/michaelis-menten/ (cit. on p. 14).

[43] Philippe Cinquin et al. «A glucose biofuel cell implanted in rats». In: *PloS one* 5.5 (2010), e10476 (cit. on p. 16).

[44] Michelle Rasmussen, Roy E Ritzmann, Irene Lee, Alan J Pollack, and Daniel Scherson. «An implantable biofuel cell for a live insect». In: *Journal of the American Chemical Society* 134.3 (2012), pp. 1458–1460 (cit. on p. 16).

[45] Lenka Halámková, Jan Halámek, Vera Bocharova, Alon Szczupak, Lital Alfonta, and Evgeny Katz. «Implanted biofuel cell operating in a living snail». In: *Journal of the American Chemical Society* 134.11 (2012), pp. 5040–5043 (cit. on p. 16).

[46] Mark Southcott, Kevin MacVittie, Jan Halámek, Lenka Halámková, William D Jemison, Robert Lobel, and Evgeny Katz. «A pacemaker powered by an implantable biofuel cell operating under conditions mimicking the human blood circulatory system–battery not included». In: *Physical chemistry chemical physics* 15.17 (2013), pp. 6278–6283 (cit. on p. 16).

[47] Fernanda CPF Sales, Rodrigo M Iost, Marccus VA Martins, Maria C Almeida, and Frank N Crespilho. «An intravenous implantable glucose/dioxygen biofuel cell with modified flexible carbon fiber electrodes». In: *Lab on a Chip* 13.3 (2013), pp. 468–474 (cit. on p. 16).

[48] RA Escalona-Villalpando, AC Martínez-Maciel, JC Espinosa-Ángeles, E Ortiz-Ortega, N Arjona, LG Arriaga, and J Ledesma-García. «Evaluation of hybrid and enzymatic nanofluidic fuel cells using 3D carbon structures». In: *International Journal of Hydrogen Energy* 43.26 (2018), pp. 11847–11852 (cit. on pp. 17, 19, 24, 70, 71).

[49] Cheong Hoon Kwon et al. «High-power biofuel cell textiles from woven biscrolled carbon nanotube yarns». In: *Nature communications* 5.1 (2014), p. 3928 (cit. on pp. 18, 19, 71).

[50] Isao Shitanda, Kai Hirano, Noya Loew, Hikari Watanabe, Masayuki Itagaki, and Tsutomu Mikawa. «High-performance, two-step/Bi-enzyme lactate biofuel cell with lactate oxidase and pyruvate oxidase». In: *Journal of Power Sources* 498 (2021), p. 229935 (cit. on pp. 19, 72).

[51] Yun Chen, Kenath Priyanka Prasad, Xuewan Wang, Hongchang Pang, Ruyu Yan, Aung Than, Mary B Chan-Park, and Peng Chen. «Enzymeless multi-sugar fuel cells with high power output based on 3D graphene–Co 3 O 4 hybrid electrodes». In: *Physical Chemistry Chemical Physics* 15.23 (2013), pp. 9170–9176 (cit. on pp. 19, 70).

[52] Belkis Atasever Arslan, Erhan Akdoğan, Fevzi Çakmak Cebeci, and Tunc Catal. «Bioelectricity generation using human neuronal-like cells in single chamber biofuel cells». In: *Journal of Cleaner Production* 271 (2020), p. 122505 (cit. on p. 22).

[53] Stefano Ferri, Katsuhiro Kojima, and Koji Sode. «Review of glucose oxidases and glucose dehydrogenases: a bird's eye view of glucose sensing enzymes». In: *Journal of diabetes science and technology* 5.5 (2011), pp. 1068–1076 (cit. on pp. 24, 49).

[54] Takeshi Sakurai and Kunishige Kataoka. «Basic and applied features of multicopper oxidases, CueO, bilirubin oxidase, and laccase». In: *The Chemical Record* 7.4 (2007), pp. 220–229 (cit. on p. 24).

[55] Jacob A Bauer, Monika Zámocká, Juraj Majtán, and Vladena Bauerová-Hlinková. «Glucose oxidase, an enzyme "Ferrari": Its structure, function, production and properties in the light of various industrial and biotechnological applications». In: *Biomolecules* 12.3 (2022), p. 472 (cit. on pp. 25, 42, 46).

[56] Fei Wu, Lei Su, Ping Yu, and Lanqun Mao. «Role of organic solvents in immobilizing fungus laccase on single-walled carbon nanotubes for improved current response in direct bioelectrocatalysis». In: *Journal of the American Chemical Society* 139.4 (2017), pp. 1565–1574 (cit. on p. 25).

[57] Takahiro Maruyama. «Carbon nanotubes». In: *Handbook of Carbon-Based Nanomaterials*. Elsevier, 2021, pp. 299–319 (cit. on p. 25).

[58] Bartłomiej Olszewski and Krzysztof Stolarczyk. «Laccase-catalyzed reduction of oxygen at electrodes modified by carbon nanotubes with adsorbed promazine or acetosyringone». In: *Catalysts* 8.10 (2018), p. 414 (cit. on p. 24).

[59] Arnaud Magrez, Sandor Kasas, Valérie Salicio, Nathalie Pasquier, Jin Won Seo, Marco Celio, Stefan Catsicas, Beat Schwaller, and László Forró. «Cellular toxicity of carbon-based nanomaterials». In: *Nano letters* 6.6 (2006), pp. 1121–1125 (cit. on p. 25).

[60] LibreTexts Chemistry. *Cyclic Voltammetry*. 2023. URL: https://chem.libretexts.org/Bookshelves/Analytical_Chemistry/Supplemental_Modules_(Analytical_Chemistry)/Instrumentation_and_Analysis/Cyclic_Voltammetry#:~:text=Cyclic%20Voltammetry%20(CV)%20is%20an,and%20measuring%20the%20resulting%20current (cit. on p. 26).

[61] Fabio Ruiz Simões and Miguel Gustavo Xavier. «Electrochemical sensors». In: *Nanoscience and its Applications* 1 (2017), pp. 155–178 (cit. on p. 27).

[62] Camilla Baj-Rossi, Giovanni De Micheli, and Sandro Carrara. «Electrochemical detection of anti-breast-cancer agents in human serum by cytochrome P450-coated carbon nanotubes». In: *Sensors* 12.5 (2012), pp. 6520–6537 (cit. on p. 28).

[63] Justyna Lipus and Katarzyna Krukiewicz. «Challenges and limitations of using charge storage capacity to assess capacitance of biomedical electrodes». In: *Measurement* 191 (2022), p. 110822 (cit. on p. 29).

[64] Yiming Yan, Wei Zheng, Lei Su, and Lanqun Mao. «Carbon-nanotube-based glucose/O2 biofuel cells». In: *Advanced Materials* 18.19 (2006), pp. 2639–2643 (cit. on p. 29).

[65] Klaus Piontek, Matteo Antorini, and Thomas Choinowski. «Crystal structure of a laccase from the fungusTrametes versicolor at 1.90-Å resolution containing a full complement of coppers». In: *Journal of Biological Chemistry* 277.40 (2002), pp. 37663–37669 (cit. on p. 41).

[66] Kyuhwan Hyun, Sang Won Han, Won-Gun Koh, and Yongchai Kwon. «Direct electrochemistry of glucose oxidase immobilized on carbon nanotube for improving glucose sensing». In: *International journal of hydrogen energy* 40.5 (2015), pp. 2199–2206 (cit. on p. 42).

[67] Cristina Boero, Sandro Carrara, Giovanna Vecchio, Laura Calzà, and Giovanni Micheli. «Highly sensitive carbon nanotube-based sensing for lactate and glucose monitoring in cell culture». In: *IEEE transactions on nanobioscience* 10.1 (2011), pp. 59–67 (cit. on p. 48).

[68] Scott Calabrese Barton, Josh Gallaway, and Plamen Atanassov. «Enzymatic biofuel cells for implantable and microscale devices». In: *Chemical reviews* 104.10 (2004), pp. 4867–4886 (cit. on p. 56).

[69] Mark Southcott, Kevin MacVittie, Jan Halámek, Lenka Halámková, William D Jemison, Robert Lobel, and Evgeny Katz. «A pacemaker powered by an implantable biofuel cell operating under conditions mimicking the human blood circulatory system–battery not included». In: *Physical chemistry chemical physics* 15.17 (2013), pp. 6278–6283 (cit. on p. 56).

[70] Nerea Casado and David Mecerreyes. «Introduction to redox polymers: Classification, characterization methods and main applications». In: (2020) (cit. on p. 58).

[71] Eduardus Ariasena, Ivandy Arifin Putra Noerrizky, Raih Rona Althof, and Isa Anshori. «Screen-Printed Carbon Electrode Fabrication Method for Electrochemical Biosensor Application». In: *4th International Conference on Life Sciences and Biotechnology (ICOLIB 2021)*. Atlantis Press. 2022, pp. 341–353 (cit. on p. 58).

[72] Tien-Fu Chu, Raja Rajendran, Iren Kuznetsova, and Gou-Jen Wang. «High-power, non-enzymatic glucose biofuel cell based on a nano/micro hybrid-structured Au anode». In: *Journal of Power Sources* 453 (2020), p. 227844 (cit. on p. 70).

[73] Fernanda CPF Sales, Rodrigo M Iost, Marccus VA Martins, Maria C Almeida, and Frank N Crespilho. «An intravenous implantable glucose/dioxygen biofuel cell with modified flexible carbon fiber electrodes». In: *Lab on a Chip* 13.3 (2013), pp. 468–474 (cit. on p. 70).

[74] Cheong Hoon Kwon, Yongmin Ko, Dongyeeb Shin, Minseong Kwon, Jinho Park, Wan Ki Bae, Seung Woo Lee, and Jinhan Cho. «High-power hybrid biofuel cells using layer-by-layer assembled glucose oxidase-coated metallic cotton fibers». In: *Nature communications* 9.1 (2018), p. 4479 (cit. on p. 71).

[75] Zepeng Kang, Kailong Jiao, Jin Cheng, Ruiyun Peng, Shuqiang Jiao, and Zongqian Hu. «A novel three-dimensional carbonized PANI1600@ CNTs network for enhanced enzymatic biofuel cell». In: *Biosensors and Bioelectronics* 101 (2018), pp. 60–65 (cit. on p. 71).

[76] Cheong Hoon Kwon et al. «High-performance hybrid biofuel cells using amphiphilic assembly based enzyme electrodes». In: *Applied Physics Reviews* 9.2 (2022) (cit. on p. 71).

[77] Ayumu Niiyama, Kazuki Murata, Yasushi Shigemori, Abdelkader Zebda, and Seiya Tsujimura. «High-performance enzymatic biofuel cell based on flexible carbon cloth modified with MgO-templated porous carbon». In: *Journal of Power Sources* 427 (2019), pp. 49–55 (cit. on p. 71).

[78] Isao Shitanda, Kotaro Takamatsu, Ayumu Niiyama, Tsutomu Mikawa, Yoshinao Hoshi, Masayuki Itagaki, and Seiya Tsujimura. «High-power lactate/O2 enzymatic biofuel cell based on carbon cloth electrodes modified with MgO-templated carbon». In: *Journal of Power Sources* 436 (2019), p. 226844 (cit. on p. 71).

[79] Ryo Suzuki, Isao Shitanda, Tatsuo Aikawa, Toshifumi Tojo, Takeshi Kondo, Seiya Tsujimura, Masayuki Itagaki, and Makoto Yuasa. «Wearable glucose/oxygen biofuel cell fabricated using modified aminoferrocene and flavin adenine dinucleotide-dependent glucose dehydrogenase on poly (glycidyl methacrylate)-grafted MgO-templated carbon». In: *Journal of Power Sources* 479 (2020), p. 228807 (cit. on p. 72).

[80] Bertrand Reuillard, Alan Le Goff, Charles Agnes, Michael Holzinger, Abdelkader Zebda, Chantal Gondran, Kamal Elouarzaki, and Serge Cosnier. «High power enzymatic biofuel cell based on naphthoquinone-mediated oxidation of glucose by glucose oxidase in a carbon nanotube 3D matrix». In: *Physical Chemistry Chemical Physics* 15.14 (2013), pp. 4892–4896 (cit. on p. 72).

[81] Leni Zhong, Lixue Tang, Shuaijian Yang, Zhenting Zhao, Zijian Zheng, and Xingyu Jiang. «Stretchable Liquid Metal-Based Metal-Polymer Conductors for Fully Screen-Printed Biofuel Cells». In: *Analytical chemistry* 94.48 (2022), pp. 16738–16745 (cit. on p. 72).

[82] Takeo Miyake, Keigo Haneda, Nobuhiro Nagai, Yohei Yatagawa, Hideyuki Onami, Syuhei Yoshino, Toshiaki Abe, and Matsuhiko Nishizawa. «Enzymatic biofuel cells designed for direct power generation from biofluids in living organisms». In: *Energy & Environmental Science* 4.12 (2011), pp. 5008–5012 (cit. on p. 72).

[83] Balamurugan Devadas, Veerappan Mani, and Shen-Ming Chen. «A glucose/O2 biofuel cell based on graphene and multiwalled carbon nanotube composite modified electrode». In: *International Journal of Electrochemical Science* 7.9 (2012), pp. 8064–8075 (cit. on p. 72).

[84] Nicolas Mano, Fei Mao, and Adam Heller. «A miniature membrane-less biofuel cell operating at+ 0.60 V under physiological conditions». In: *ChemBioChem* 5.12 (2004), pp. 1703–1705 (cit. on p. 72).

Appendix A

Biofuel cell comparison

Table A.1: Literature review

REFERENCE	FUEL	POWER DENSITY [$\mu W/cm^2$]	VOLTAGE [V]	MATERIAL	TYPE	OPERATIVE CONDITIONS	APPLICATION
Tien-Fu Chu et al. [72]	500 mM of Glucose	10700	0.36	Anode: Au thin film on polycarbonate. Cathode: graphene film coated glassy carbon electrode	Abiotic	pH = 14 T = 23 °C	Not defined
A.Zebda et al. [4]	Glucose (physiological concentration)	193.5	Not mentioned (OCP = 0.57V)	Carbon nanotubes on pellet bioelectrodes	Enzymatic: Glucose oxidase with catalase at anode and Laccase at cathode	Physiological	Implanted in the abdominal cavity of a rat
A. Zebda et al. [40]	5 mM of Glucose in air saturated buffer solution	1'000	0.65	Compressed Multi Wallet carbon nanotubes	Enzymatic: Glucose oxidase with catalase at anode and Laccase at cathode	pH = 7 T = 23 °C	Progress in powering medical devices
F.Sales et al. [73]	47 mM of Glucose in buffer solution	200	0.250	Carbon fibers at anode and carbon fibers modified with platinum nanoparticles at cathode.	Enzymatic with MET at anode (glucose oxidase and mediator) and abiotic at cathode	pH = 7.2 T = 23 °C	Progress in powering medical devices
F.Sales et al. [73]	In vivo (physiological concentration)	95	0.08	Carbon fibers at anode and carbon fibers modified with platinum nanoparticles at cathode	Enzymatic with MET at anode (glucose oxidase and mediator) and abiotic at cathode	Physiological	Inserted into jugular vein of a living rat
Y. Chen et al. [51]	200 mM Glucose, 50 mM Sucrose, 100 mM Lactose	2375	0.4	3D graphene Co304 and Nafion in between	Abiotic	pH = 5 Mild temperature. Separated anodic and cathodic chamber	Next generation powering devices
R.A. Escalona-Villalpando et al. [48]	5 mM of Glucose at anode, oxygen saturated solution at cathode	5700	0.29	Carbon nanofoam. At cathode spray-coated with Pt	Enzymatic at anode (glucose oxidase) and hybrid at cathode	pH = 7.1 T = 23°C Separated anodic and cathodic chamber	Miniaturized nanofluidic power sources

R.A. Escalona-Villalpando et al. [48]	5 mM of Glucose at anode, oxygen saturated solution at cathode	17000	0.51	Carbon nanofoam. At anode spray-coated with AuAg/C	Enzymatic at cathode (laccase) and abiotic at anode	pH = 5 T = 23°C Separated anodic and cathodic chamber	Miniaturized nanofluidic power sources
R.A. Escalona-Villalpando et al. [48]	5 mM of glucose at anode, oxygen saturated solution at cathode	3200	0.25	Carbon nanofoam	Enzymatic: glucose oxidase at anode and laccase at cathode	pH = 7.1 T = 23°C Separated anodic and cathodic chamber	Miniaturized nanofluidic power source
K.Cheong Hoon et al. [49]	Human sierum	1020	0.36	Multi-wallet carbon nanotubes	Enzymatic: glucose oxidase at anode (MET) and bilirubin oxidase at cathode (MET)	Physiological	Powering medical devices
K.Cheong Hoon et al. [74]	300mM of Glucose	3700	0.4	Metallic cotton fiber based	Enzymatic at anode (glucose oxidase), abiotic at cathode	pH = 7.4 T = 36.5	final purpose is to be implantable
K. Zepeng et al. [75]	100mM of Glucose	1120	0.45	Carbonized composite of PANI@CNTs. Nafion membrane	Enzymatic: glucose oxidase at anode and Laccase at cathode	pH = 5 T = 25°C Anode and cathode in two different compartments	Not defined
K.Cheong Hoon et al. [76]	300 mM of Glucose	7300	0.5	Cotton fiber based at anode. Cotton fiber with Pt at cathode.	Enzymatic at anode (glucose oxidase) and abiotic at cathode	pH = 7.4 T = 36.5 °C	Not defined
B.I. Rapoport et al.[5]	10 mM of Glucose	180	0.18	Platinum at anode, Single walled carbon nanotubes	Abiotic	pH = 7.4 T = 24°C	Powering brain-machine interface from interstitial fluid
A. Niiyama et al. [77]	1M of Glucose	2000	0.4	MgO-templated carbon	Enzymatic (MET): FAD-GDH and mediator at anode and bilirubin oxidase and mediator at cathode	pH = 7 T = 23°C Two different containers	Not defined
I. Shitanda et al. [78]	20 mM of Lactate	1000	0.5	Carbon cloths electrodes modifies with MgOC	Enzymatic: lactate oxidase and mediator at anode and bilirubin oxidase and mediator at cathode	pH = 7 T = 23°C	Wearable application

B. Amay J. et al. [6]	20 mM of Lactate	1200	0.2	Au layer functionalized with CNT at anode and Au layer functionalized with CNT silver oxide at cathode	Enzymatic (MET) at anode with lactate oxidase. Abiotic at cathode	human sweat	Able to power a BLE radio and to turn on a LED
I. Shitanda et al. [50]	200 mM of Lactate	1750	0.35	Porous carbon-impregnated carbon cloth	Enzymatic: Lactate oxidase and pyruvate oxidase at anode. Bilirubin oxidase at cathode.	pH = 7 T = 23 °C	Enzymatic cascade in biofuel cell
R. Suzuki et al. [79]	300 mM of Glucose	3600	0.45	MgOC modified carbon cloth	Enzymatic: FAD-GDH and mediator at anode; and bilirubin oxidase at cathode	pH = 7 T = 25 °C	Power of medical devices
R. Bertrand et al. [80]	50 mM in buffer solution air saturated	1100	0.5	Multi Walled Carbon nanotubes	Enzymatic: Glucose oxidase at anode with mediator and laccase at cathode	pH = 7 T = 40°C	Power a LED
Z. Leni et al. [81]	0.2 mM of Glucose	14	0.31	Carbon based	Glucose oxidase at anode and bilirubin oxidase at cathode	pH = 7 T = 23°C	Power a LED, harvesting energy from sweat
S. Philipp et al. [25]	0.5 M of Glucose	43	0.06	Platinum based with CeO2 membrane	Abiotic	pH = 7 T = 37 °C	Implantable biofuel cell
T. Miyake et al. [82]	Physiological glucose condition while oxygen collected from air	131.25	0.56	Conductive polymer based	Enzymatic (MET): GDH and mediator at anode; bilirubin oxidase at cathode	Rat blood	Implanted in a rat vein
B. Devadas et al. [83]	10 mM of Glucose, O2 saturated condition	46	0.1	Graphene oxide-multiwalled carbon nanotubes at anode, graphene-Pt modified glassy carbon electrode	Enzymatic at anode: glucose oxidase with mediator; abiotic at cathode	pH = 7 T = 23°C	Not defined
N. Mano et al. [84]	15 mM of Glucose,	480	0.6	Conductive polymer based	Enzymatic: glucose oxidase at anode and bilirubin oxidase at cathode	pH = 7.2 T = 37.5 °C	Future implantable devices
M. Cadet et al. [28]	8.22 mM of Glucose (in vitro in human blood)	129	0.38	Redox polymer on carbon fiber	Enzymatic: GDH at anode and bilirubin oxidase at cathode	Physiological. Shear stress taken into account	Biofuel cell implantable in human blood